LRP 676/00 August 2000

Effect of $\mathbf{E} \times \mathbf{B}$ flows on global linear microinstabilities

M. Maccio

ISSN 0458-5895

Effect of $E \times B$ Flows on Global Linear Microinstabilities

PhD Thesis

Thesis Candidate: Matteo Maccio

Thesis Director: MER L. Villard

Centre de Recherches en Physique des Plasmas,

Association Euratom-Confédération Suisse,

Ecole Polytechnique Fédérale de Lausanne,

CRPP-PPB, CH-1015 Lausanne, Switzerland

Abstract

One of the key issues to achieve magnetically controlled fusion in tokamaks is the problem of energy and particles confinement. In the last ten years, a great deal of work has been done to study the poloidal rotations of the plasma that are induced by strong equilibrium electric fields. It is indeed observed that these rotations improve the energy and particles confinement.

It is theoretically widely believed that microinstabilities are the source of the anomalous transport. The question of how strong equilibrium electric fields affect microinstabilities must thus be addressed. We undertook the study of this phenomenon using a kinetic, linear, spectral code, resolving the full two-dimensional poloidal plane.

Results show that $E \times B$ rotations have a strong stabilizing effect on microinstabilities. Moreover, a study of the stabilization mechanism has allowed us to discover that the value of the equilibrium electric field is as important as the value of its first derivative. We also observed that the second derivative does not exhibit any relevant effect.

We then studied the combined effect of $E \times B$ rotations and negative magnetic shears. The results did not show any particular behavior of the negative magnetic shear cases. Eventually, we conducted an experimental comparison with the Asdex Upgrade tokamak in Garching.

Version abrégée

La question du confinement des particules et de l'énérgie dans les tokamaks est cruciale pour la réussite du projet de la fusion. Au cours de la dernière décennie, un grand intérêt a été porté aux rotations poloïdales du plasma, dues à de forts champs éléctriques d'équilibre. On observe en effet, qu'en présence de ces rotations, le confinement des particules et de l'énérgie est fortement amélioré.

Il est théoriquement et généralement admis que les microinstabilités sont à l'origine du transport anormal. La question de savoir comment les forts champs éléctriques d'equilibre influent sur les microinstabilités est donc intéressante. Nous avons entrepris d'étudier ce phénomène au moyen d'un code cinétique, linéaire, spectral et résolvant les deux dimensions du plan poloïdal.

Les résultats montrent que que les rotations $E \times B$ ont un fort effet stabilisant sur les microinstabilités. Par ailleurs, une étude relative au mécanisme de stabilisation a permis de constater que la valeur du champ éléctrique est aussi importante que la valeur de sa première dérivée. Par contre, la seconde dérivée semble n'avoir aucun effet.

Nous avons également étudié l'effet des rotations $E \times B$ au cours d'une inversion du cisaillement magnétique. Cela n'a permis de distinguer aucun comportement particulier des cas à cisaillement négatif. Pour finir, une comparaison expérimentale avec le tokamak Asdex Upgrade de Garching a été menée à bien.

Contents

Chapter 1

Introduction

1.1 For the Innocent Eye

The wish for a clean and inexhaustible source of energy has led man to study the process called "fusion". Fusion is the reaction by which two light atoms combine to form a heavier one, releasing a large amount of energy along the way. There are many such reactions, one example being:

$$D + D \rightarrow He^3 + n \tag{1.1}$$

where two deuterium (D) atoms combine to produce a helium (He^3) atom and a fast neutron (n). Here we see why fusion is an excellent candidate to be a "clean and inexhaustible" source of energy. Indeed, only deuterium is needed as an input and it is widely available among the oceans for millions of years. Moreover, the reaction produces helium, which is a neutral gas, and a fast neutron, which is the real source of the energy. None of these is polluting.

So far, so good, but as everyone knows, there is no such thing as a free lunch. Where does the problem lurk ? Well, reactions such as (1.1) take place at the enjoyable room temperature, but only very slowly. In order to recover some useful energy, the reaction must be heated to the not so enjoyable temperature of several million degrees. And here come the problems: how do you store anything so hot ?

Physicists have thought of different solutions. The one of interest for us is called "magnetic confinement". The idea is simple: at the given temperature of several

million degrees, all atoms are ionized, which means that electrons are split from the kernel of neutrons and protons. This fact has an interesting consequence: the gas becomes a plasma, that is a bath of charged particles. And here comes the idea: as charged particles see magnetic fields, why not try to create a "magnetic bottle" ? That is precisely one of the solutions which is currently tried worldwide.

As physicists are highly creative creatures, the "magnetic bottles" come in various shapes and sizes. The one which will entertain us for the following tens of pages is called "tokamak" and to put it simply, would look, if you could see magnetic fields, like a tire.

But this is not the end of the story: these magnetic bottles, whatever their shape and size, are never perfectly waterproof. This means there is a loss of particles and energy. Unfortunately, it is more than a minor defect: up to now it has prevented fusion plasmas to burn on their own. In other words, it has not yet been possible to have an output of energy larger than the input with a fusion reaction. Well, the previous statement is not quite true: it has been possible, but only without control, that is with the hydrogen bomb. But this is another story.

What you still need to know is that this transport of energy and particles is not well explained by classical theories and is thus called "anomalous". It is believed to be caused by some unstable eigenmodes of the plasma, which are called micro-instabilities. But micro-instabilities are by no means easy to observe in experiments, thus we only have theoretical conjectures for the moment.

However, in recent years experiments have shown that the creation of internal transport barriers can strongly reduce this anomalous transport. How these transport barriers are generated is not very clear, but a wide consensus attribute them to the existence of a strong radial electric field in the plasma. Although there is some experimental evidence of this, no theoretical model explains simply the mechanism by which the strong electric field can reduce transport.

At this point you should know enough to ask yourself: if strong radial elec-

tric fields reduce the anomalous transport, which is supposedly caused by micro-instabilities, could we investigate with theoretical tools the effect of the strong electric field on the micro-instabilities ? There we are: it is what we have tried to do in this PhD work, with two simple models and a somehow reduced physics.

1.2 To Get More into the Details

As written in the first part, which was intended for the non specialist reader, micro-instabilities such as the Ion Temperature Gradient (ITG) modes, the Trapped Ion or Electron Modes (TIM and TEM) are widely held responsible for the anomalous transport observed in tokamaks. These modes can get unstable using the free energy available in the system, which arises from the inhomogeneities of the plasma. The linear stability of these modes has been thoroughly studied, first through dispersion relations [1]-[2], then with ballooning representations [3]-[7] and eventually with global codes [8]-[10]

As also already said, some evidence has been recently noticed that $E \times B$ flows could be responsible for the creation of Internal Transport Barriers (ITB) in tokamaks, thus improving the confinement [11]. If so, the $E \times B$ flows should strongly affect the spectrum of micro-instabilities. There are many questions related to $E \times B$ flows, for instance, how is in first place generated the strong radial electric field ? or how do the non-linear saturation mechanism lead to a new steady state of the plasma with $E \times B$ flows ? We have decided to address a very modest problem: how do ad hoc $E \times B$ flows affect the linear stability of micro-instabilities ? No matter how simple this question is, it is nevertheless not too simple and allowed us to answer some interesting questions, as will be presented later.

Let us begin with a short history of our subject. Detailed informations about experimental results are to be found in Burrell's review papers [11]-[13] and in Connor's review paper [14]. These can also serve as excellent general references for theory papers. First attempts to study the effect of $E \times B$ flows on ITG modes

include a linear kinetic model in slab sheared geometry by Staebler and Dominguez [15]. They observed a stabilization of the ITG modes and claimed a strong influence of both the first and the second derivative of the radial electric field. Following attempts include an hydrodynamic model in slab geometry by Wang, Diamond and Rosenbluth [16]. Their main result is that a weak sheared flow is destabilizing, but that strong flows are stabilizing. Their analysis also resulted in the insensitivity of stabilization to the sign of the first derivative of the flow. Non-linear calculations to study the generation of $E \times B$ flows and the saturation mechanisms were first performed by Cohen et al [17]. They used a partially linearized δf algorithm in a shear slab geometry. They also found a stabilization for strong flows, independent of the sign of the first derivative, though weakly depending on the sign of the second derivative of flow. Ballooning simulations include Waltz and al. [18] and Rewoldt and al.[19], although it must be stressed that Taylor and Wilson [20] have proven that ballooning transform does not apply formally in the case of a plasma with an $E \times B$ flow. Moreover, there have been insisting claims by Sen et al. [21], [22] that the only relevant effect in the flow profile is its second derivative. They find that the first derivative of the $E \times B$ flow is unimportant. Study of the decorrelation induced by $E \times B$ flows has been done by Hahm and Burrell [23]-[25]. A discussion of the Kelvin-Helmholtz instability can be found in G. Ganguli. He explains that Landau damping prevents these instabilities from bothering us [26].

The last work that we would like to cite is the closest to our own work: in 1996 Kim and Kishimoto [27] investigated the effect of sheared $E \times B$ flows on the toroidal branch of the ITG modes, using a global linear PIC code with kinetic ions and adiabatic electrons. They found that the sheared rotation of the plasma induced a rotation of the ITG mode and a consecutive stabilization of the mode. They concluded that the stabilization mechanism for the toroidal ITG modes and the slab-like ones were very different. We will later see that our results fully agree with their observations and interpretations, but extend their results as we explored

also non-sheared $E \times B$ flows. Nevertheless, they were the first to point out the qualitative difference that exists between the stabilization mechanisms of the slab and toroidal ITG modes.

A much larger literature is available, including several papers on the effect of a toroidal rotation of the plasma or on the influence of the $E \times B$ flows on edge turbulence, but as they are not directly related to our work, we decided to not mention them.

As we see, there has been already a lot of work done. There remain still some questions that have not been answered satisfactorily. For instance, what is the main stabilizing mechanism ? What is relevant in the profile of flow: its first derivative, its second derivative or maybe its value ? As most of the models so far addressed only a slab geometry, the qualitative difference in how $E \times B$ flows affect toroidal and slab ITG modes is to be more extensively studied. We have tried to address these questions with two different physical models: a fluid model and a gyrokinetic one, both being linear, spectral, electrostatic and solving the full 2-dimensional poloidal plane. Our first approach was a simple set of equations where we had an ion fluid and adiabatic electrons [28]. This had a strong drawback: the lack of Landau damping allowed plenty of unstable slab-like ITG modes to exist even in the tokamak geometry. The slab-like modes being almost not affected by the $E \times B$ flows, the results of the fluid model were rather disappointing, although a strong effect on the toroidal ITG modes could be seen, it was not possible to study it in details. Our second attempt was much more rewarding: we took Hahm's [29] gyrokinetic equation in the presence of a strong radial electric field and solved it using the formalism developed by Brunner et al. [10]. This formalism solves the problem of the linear stability of ITG, TIM and TEM modes in the full 2-dimensional poloidal plane. It includes the effects of finite Larmor radius (FLR) to all orders in a spectral approach. The results were much more interesting this time.

1.3 The Results

First of all, let me summarize what is the understood mechanism by which strong radial electric fields reduce the anomalous transport [11]. If the $E \times B$ rotation, induced by the radial electric field, is *sheared*, then it should *decorrelate* the instability, thus reducing it [14]. A generally accepted estimation of the "shearness" of the flow is:

$$\gamma_{E\times B} = \left(\frac{\Delta\rho_o}{\Delta\theta}\right) \partial_\rho \left(\frac{u(\rho)}{\rho}\right) \tag{1.2}$$

where $\Delta\rho_o$ and $\rho\Delta\theta$ are the correlation of the ambient turbulence in the radial and poloidal directions respectively, $u(\rho)$ is the poloidal velocity and ρ is the minor radius.

We will show that there is also a second mechanism of stabilization that is at least as strong as this one. This mechanism is not due to the shear of the radial electric field, but to its actual value where the mode localizes. To give a brief explanation, this second mechanism works as follows: the fact that the poloidal rotation of the plasma is non vanishing at the radial position where the mode localizes induces a rotation of the mode. But, as for toroidal ITG modes, their main drive comes through the region of unfavorable curvature of the magnetic field. Thus, if the mode is removed from this region, its drive is reduced and it gets stabilized.

Still with an ITG mode, we studied another phenomenon, which is usually summoned to explain ITB: the inversion of magnetic shear. Although Brunner [10] showed that this had no dramatic effect on linear micro-instabilities, we have included a study of this effect combined with poloidal flows. Our results will show that, in a linear model, no great synergy between $E \times B$ flows and negative magnetic shear can be observed. Indeed, the effect of flows will be seen as the strongest on positive magnetic shear cases.

Besides, we have also made a comparison with a shot from the Asdex Upgrade (AUG) tokamak in Garching. In this ITB shot, we took the experimental profiles

for all the equilibrium quantities, including the radial electric field, and found a good agreement between our calculations and the experimental data. Of course, as our model is very simple (for instance, it misses the electromagnetic effects), this agreement might be more due to luck than to good physics. A definitive answer to this doubt can only brought by simulating more experimental shots.

1.4 Structure of the Work

After this introduction, you will find the fluid model, whose equations and results have been cast in the single chapter two, as they were not very interesting. In chapter three, the gyrokinetic equations will be presented, first in a general geometry, then in the special case of a tokamak with passing particles first and trapped particles then. A short discussion of the numerical implementation follows. Chapter four contains the core of this work, the gyrokinetic results. Finally, a conclusion will put an end to this four years work.

Chapter 2

Fluid Model and Results

Let us begin with the fluid model. Although the results were not thrilling, this model was important to me for two reasons: it was my first contact with the micro-instabilities plasma physics and my first contact with numerical methods and their coding on computers. Besides, it was the first attempt to address globally the study of the effect of $E \times B$ flows on linear ITG modes.

2.1 Equations

The plasma is modeled by an ion fluid and adiabatic electrons. Considering electrostatic perturbations the system is closed using the quasi-neutrality condition. The equations are simplified using the gyrokinetic ordering [29] and resolved globally within a spectral approach.

The ion fluid is described by the equations of continuity and motion (without viscosity) that are closed assuming that the perturbed pressure is isobaric. Moreover, we assume an ad hoc equilibrium state; this allows us to choose arbitrary profiles for ion equilibrium pressure, electron temperature and density and to assume that the time dependence of the perturbed quantities is $\exp(-i\omega t)$ with $\omega \in \mathbb{C}$, the so-called

spectral approach. Our equations read:

$$i\omega\phi = \frac{T_e}{n_0 e}\nabla\cdot(n_0\mathbf{v}) \tag{2.1}$$

$$i\omega p = \frac{1}{B}[\nabla\phi\times\nabla p_0]\cdot\mathbf{e}_{\|} \tag{2.2}$$

$$i\omega v_{\|} = \frac{1}{m_i n_0}\partial_{\|}p + \frac{e}{m_i}\partial_{\|}\phi \tag{2.3}$$

$$\mathbf{v} = v_{\|}\mathbf{e}_{\|} + \frac{1}{B}\left[\mathbf{e}_{\|}\times\nabla\phi + i\frac{\omega}{\omega_{ci}}\nabla_{\perp}\phi\right] + \frac{1}{eBn_0}\mathbf{e}_{\|}\times\nabla p \tag{2.4}$$

Equation (2.1) is the continuity equation coupled with the quasi-neutrality condition, where ϕ is the electrostatic perturbation, T_e is the electron temperature, n_0 is the equilibrium density, e is the proton charge and $\mathbf{v}$ is the fluid velocity. Equation (2.2) is the closure equation, where p is the perturbed pressure, B is the modulus of the magnetic field, p_0 is the equilibrium pressure and $\mathbf{e}_{\|} = \mathbf{B}/B$. Equations (2.3) and (2.4) are the equations of motion, where $v_{\|}$ is the perturbed parallel velocity, m_i is the ion mass, $\partial_{\|} = (\mathbf{e}_{\|}\cdot\nabla)$, $\nabla_{\perp} = \nabla - \mathbf{e}_{\|}(\partial_{\|})$ and $\omega_{ci} = eB/m_i$ is the ion-cyclotron frequency. Equation (2.4) has to be inserted in equation (2.1) and then Eqs. (2.1)-(2.3) form a complete system for the unknowns $\{\phi, v_{\|}, p\}$.

So far our equations are valid whatever the geometry is, but in order to include the sheared poloidal flow we now restrict ourselves to large aspect ratio tokamaks. We assume a very simple geometry: concentric circular flux surfaces, with the following magnetic field:

$$\mathbf{B} = \frac{R}{r(\rho)}B_0\left(\mathbf{e}_{\varphi} + \frac{\rho}{Rq_s(\rho)}\mathbf{e}_{\theta}\right) \tag{2.5}$$

where R is the major radius, $r(\rho) = R + \rho\cos(\theta)$ is the cylindrical radius, B_0 is the magnetic field on the axis, $\mathbf{e}_{\varphi}$ is the unit vector along the toroidal angle, $\rho\in[0,a]$ is the minor radius, $q_s(\rho)$ is the safety factor, which is chosen arbitrarily, and $\mathbf{e}_{\theta}$ is the unit vector along the poloidal angle. We assume that $a/R \ll 1$.

We now introduce the poloidal sheared $E\times B$ flow by assuming that our equilibrium state does have a poloidal sheared rotation $u_{\theta}(\rho)\mathbf{e}_{\theta}$. This equilibrium velocity can be chosen arbitrarily. Moreover, we retain it only on the left-hand

side of Eqs.(2.1)-(2.3), which corresponds to retaining only the leading contribution in the Hahm kinetic equations [29]. Thus, the effect of flow is to transform $i\omega \rightarrow i \cdot \omega - u_\theta(\rho)(\frac{1}{\rho}\partial_\theta)$ in the left-hand side of Eqs.(2.1)-(2.3). The flow profile is normalized with respect to the ion thermal velocity multiplied by a Mach number, i.e. $u_\theta(\rho) = \text{Mach} \cdot v_{thi} \cdot \tilde{u}_\theta(\rho)$ with $\tilde{u}_\theta(\rho) \in [-1, 1]$.

We may write the local dispersion relation, including sheared poloidal flow as:

$$0 = 1 + \frac{\omega_n^*}{\omega - k_\theta u_\theta} + \left[1 - \frac{\omega_p^*}{\omega - k_\theta u_\theta}\right]\left[(k_\perp \rho_L^*)^2 - \left(\frac{k_\parallel c_s}{\omega - k_\theta u_\theta}\right)^2 + \frac{< \omega_{gi} >}{\omega - k_\theta u_\theta}\right] \quad (2.6)$$

where $\omega_n^* = (c_s^2 k_\theta/\omega_{ci})(dln(n_0)/d\rho)$, with $c_s^2 = T_e/m_i$, $\omega_p^* = (c_s^2 k_\theta/\omega_{ci})(dln(p_0)/d\rho)$, $\rho_L^* = c_s/\omega_{ci}$, $k_\theta = m/\rho_0$ (with m being the poloidal wave number) and $< \omega_{gi} >= (2c_s^2 k_\theta/R\omega_{ci})$ is the average magnetic drift frequency. Each quantity is evaluated at some local point ρ_0. We can see, by looking at (2.6) that the effect of u_θ in the dispersion relation can only be to shift the real part of ω, i.e. changing the frequency, but not the growth rate of the instability. Therefore, the effect of u_θ cannot be interpreted locally and really requires a global resolution of the equations.

2.2 Numerical Implementation

We come now to the numerical resolution of the equations. First of all, we cast the (2.1)-(2.3) set of equations in a variational form. By this we mean the following procedure: first multiply each equation (2.1)-(2.3) with an arbitrary function (respectively $\tilde{\phi}$, $\tilde{p}$ and $\tilde{v}_\parallel$). Then integrate each equation over the whole plasma, integrating by parts and using the Gauss theorem. As is evident from a physical standpoint, we impose the Dirichlet border conditions on the electrostatic perturbation and choose the $\{\tilde{\phi}, \tilde{p}, \tilde{v}_\parallel\}$ functions such that every written symbol makes sense

and is well defined. The resulting equations are:

$$\begin{aligned}
\omega \int_\Omega \left[\frac{en_0}{T_e}\phi\tilde{\phi} + \frac{n_0}{B\omega_{ci}}\nabla_\perp\phi\cdot\nabla_\perp\tilde{\phi}\right] dx &= \int_\Omega \left[in_0 v_\parallel \nabla\tilde{\phi} + i\frac{n_0}{B}\nabla\phi\times\nabla\tilde{\phi}\cdot\mathbf{e}_\parallel\right] dx \\
&\quad + \int_\Omega \left[i\frac{1}{eB}\nabla p\times\nabla\tilde{\phi}\cdot\mathbf{e}_\parallel\right] dx \\
\omega \int_\Omega [p\tilde{p}]\, dx &= \int_\Omega \left[i\frac{1}{B}\tilde{p}\nabla p_0\times\nabla\phi\cdot\mathbf{e}_\parallel\right] dx \qquad (2.7)\\
\omega \int_\Omega [v_\parallel\tilde{v}_\parallel]\, dx &= \int_\Omega \left[-i\frac{1}{m_i n_0}\tilde{v}_\parallel\nabla_\parallel p - i\frac{e}{m_i}\tilde{v}_\parallel\nabla_\parallel\phi\right] dx
\end{aligned}$$

where Ω stands for the whole plasma and x stands for $\rho R d\rho d\theta d\varphi$.

The following step is the use of linear finite elements. This means that we are restricting the functional space in which we choose the $\{\tilde{\phi}, \tilde{p}, \tilde{v}_\parallel\}$. As we have restricted the set of equations (2.1)-(2.3) to the (2.5) geometry (in which the φ angle is ignorable), we use the following ansatz:

$$f(\rho,\theta,\varphi,t) = \sum_{k=1}^{N}\sum_{m\in\mathbb{Z}} f_{mk}\exp(+im\theta + in\varphi - iwt)\psi_k(\rho) \qquad (2.8)$$

$$\tilde{f}(\rho,\theta,\varphi,t) = \sum_{k=1}^{N}\sum_{m\in\mathbb{Z}} \tilde{f}_{mk}\exp(-im\theta - in\varphi + iwt)\psi_k(\rho) \qquad (2.9)$$

where $f \in \{\phi, p, v_\parallel\}$ and $\tilde{f} \in \{\tilde{\phi}, \tilde{p}, \tilde{v}_\parallel\}$ and $n \in \mathbb{Z}$ is fixed. The $\psi_k(\rho)$ are the basis functions that we choose as linear finite elements on a regular mesh. The f_{mk} and $\tilde{f}_{mk}$ are the unknowns to be computed.

The last step is to substitute (2.8) and (2.9) in (2.7), which leads to the a generalized eigenvalue problem:

$$Ay = B\omega y \qquad (2.10)$$

where A and B are real matrices, ω is the generalized eigenvalue and y is the corresponding eigenmode. It includes the three set of unknowns $\{\phi_{mk},\ v_{\parallel mk},\ p_{mk}\}$. This discrete form allows a resolution of the complete spectrum of the instability. The implementation of the equations was done in Fortran 90, using Lapack routines. The code was tested and run on the following platforms: on the Silicon Graphics R10000 processor, on the Sun Microsystems Sparc Ultra-2 processor and on the Cray J90

supercomputer processor. A typical run (to determine the whole spectrum) lasts between 15 minutes to 1 hour on a workstation.

We did a few validations of our code, the most important being a benchmark in a special case: given the appropriate equilibrium profiles, the analytical equations reduce to the Bessel equation, which allowed us to have a hard test of convergence for our code. A softer benchmark was the comparison with the dispersion relation (2.6): without including the $E \times B$ flows, the discrepancy between the local dispersion relation and our global code was of 10% to 20%, as expected from Brunner's work.

Now that we have a code and confidence in it, let us see what the results are.

2.3 Results

Let us first describe a typical result ($a = 0.5$ [m], $R = 2$ [m], $B = 1$ [Tesla], $n = 5$, $Te = Ti = 7.5$ [keV], $q_s(\rho) \in [1, 7]$ and $q_s \approx 4$ where the mode amplitude is maximum), without flow. The spectrum of the instability has some recurrent patterns. It has many unstable modes and it is possible to divide it into two different sorts: the slab-like and the toroidal modes, as shown in Fig.2.1. The slab-like

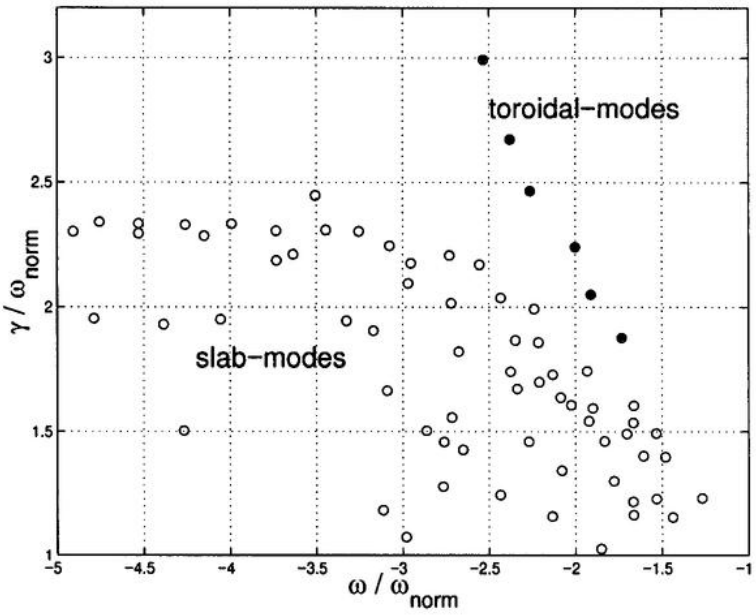

Figure 2.1: Part of the spectrum for a typical case, $\omega_{norm} = \frac{c_s^2}{a^2 \omega_{ci}}$

modes are the ones that "survive" to a cylindrical limit ($R \to \infty$ with $Rq_s(\rho)$ and $nq_s(\rho)$ being fixed), while toroidal modes need the curvature of magnetic field to exist and disappear in a cylindrical limit. As seen in Fig.2.1, there are many slab modes and just a few toroidal ones. This is a feature of the fluid model, which misses Landau damping that would stabilize most of these slab-like modes. The qualitative difference between toroidal and slab-like ITG modes is to be seen in Fig.2.2, where we have plotted the most unstable toroidal and slab-like modes.

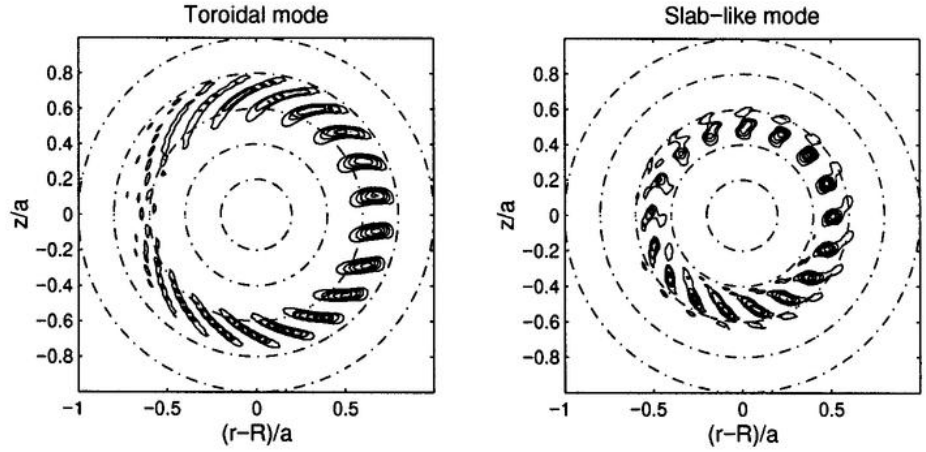

Figure 2.2: Poloidal shape of the most unstable slab-like and toroidal modes

Clearly the toroidal mode does balloon, that is it localizes in the region of unfavorable magnetic curvature, while the slab-like mode is only weakly sensitive to the magnetic curvature. This is easily understood by looking at Eq.(2.6): the slab-like mode does only need the $\left(k_{\|}c_s\right)^2$ term to exist, while the toroidal mode does need the $< \omega_{gi} >$ term (which is the average magnetic drift frequency) to exist.

Including poloidal flow strongly stabilizes the toroidal modes, but only weakly affects the slab-like modes. Even with very small values of Mach number, poloidal flow tears the toroidal modes apart and stabilizes them. As seen in Fig.2.3, the toroidal modes are strongly stabilized and disappear before Mach number reaches 0.1; in fact, in this figure, only the first four modes are toroidal ones, the others are slab-like ones. But after toroidal modes have been suppressed, the slab-like ones are still unstable and they are not too much affected by poloidal flow. Therefore, as an

artifact of our fluid model (absence of Landau damping), the maximum stabilization that can be observed mainly depends on the gap that exists between slab and toroidal modes in the absence of flow.

As the effect of flow is weak on slab-like modes and as the spectrum always contains plenty of such modes, we have never been able to observe complete stabilization of all ITG modes. Therefore, it must be stressed that the criterium $\gamma_{E\times B} \approx \gamma_{max}$ (Eq. 1.2) for full stabilization does not fit our model, as can be seen in Fig.2.3. The value of $\gamma_{E\times B}$ being a function of Mach number, we have plotted a line at the value

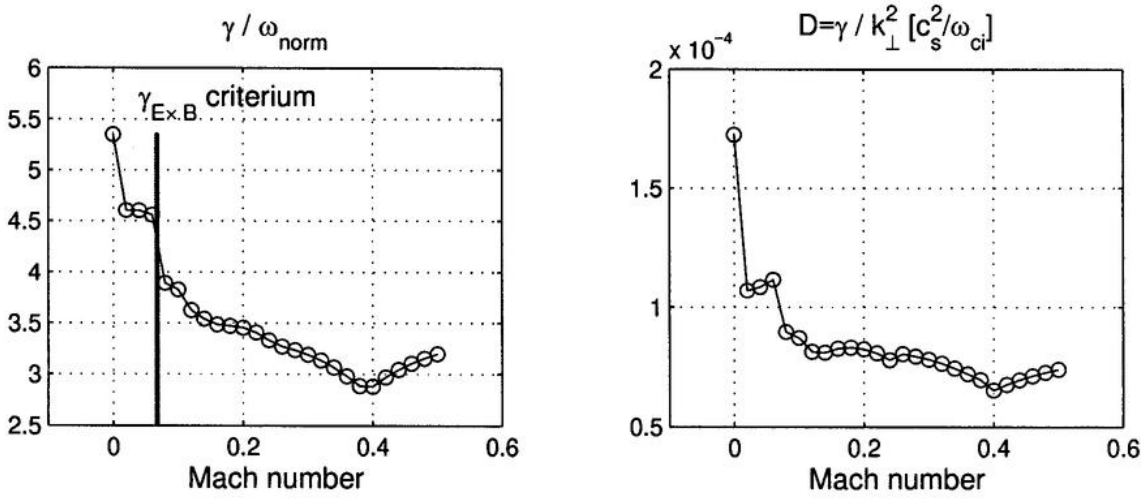

Figure 2.3: Effect of poloidal flow.

of Mach number for which $\gamma_{E\times B} = \gamma_{max}$, i.e. there should be no more unstable modes beyond this line if the criterium was to be true. In order to evaluate $\gamma_{E\times B}$, we have used $\Delta\rho_0 = k_\rho$ and $\rho\Delta\theta = k_\theta$, where $\{k_\rho, k_\theta\}$ are averaged over the most unstable mode.

Nevertheless, the poloidal flow does not only have an effect on the growth rate of the mode, but also strongly affects its radial structure, diminishing the extent of the convective cells. Therefore it exhibits two different behaviors, both tending to reduce transport. A linear estimate for the transport coefficient $D = \gamma/k_\perp^2$ is shown in Fig.2.3, where D is reduced by more than a factor two. To compute D, we average $k_\perp$ over the mode, i.e. $k_\perp^2 = \langle \nabla_\perp \phi^\star \cdot \nabla_\perp \phi \rangle / \langle \phi^\star \phi \rangle$.

We have investigated different shapes for the profile of poloidal flow and have observed that the final overall stabilization of the instability is not strongly dependent on the shape of this profile. But qualitatively, the structure of the mode strongly depends on the shape of the profile. An example is provided by the comparison of a flow which is zero where the mode amplitude is maximal (radially) but has shear there, with a flow which is non-vanishing where the mode amplitude is maximal and has the same shear. In the first case, one observes a "tilt" of the mode around the point where the flow is zero ("tilt" in the poloidal plane). In the second case, one observes a shift of the ballooning region, in the direction of rotation of the plasma (shift in the poloidal plane). Thus, as the mode without flow has no up-down symmetry, the effect of flow is also not symmetric with respect to a change in sign of Mach number. It is important also to remember that the different profiles could not be investigated in great detail, as the toroidal modes were lost into the slab modes sea, already for small values of Mach number.

We can also say that the main drives for stabilization in our model are the value and the first derivative of $u_\theta(\rho)/\rho$. The second derivative of this quantity (the so-called curvature of effective flow) is irrelevant, and this is irrespective of its sign.

We have also studied the effect of negative magnetic shear with or without flow. The scan in magnetic shear has been done like this: fix a point ρ_0 where the mode amplitude is radially maximal, fix the value of $q_s(\rho_0)$ and vary the q_s profile in order to change value of $(\rho_0 d_\rho q_s(\rho_0))/q_s(\rho_0)$. The magnetic shear does not exhibit a systematic effect (see Fig.2.4), it does stabilizes very quickly a single toroidal mode, but at the same time it is destabilizing another one. This kind of behavior seems recurrent and does not result in an overall stabilization. Nevertheless, the transport coefficient D is more smoothly affected (see Fig.2.4); it is slightly smaller for negative than for positive shear; its highest value is met by the shearless case.

The combined effects of magnetic shear and poloidal flows are shown in Fig.2.5. The first line shows the evolution of the overall maximum growth rate, for the values

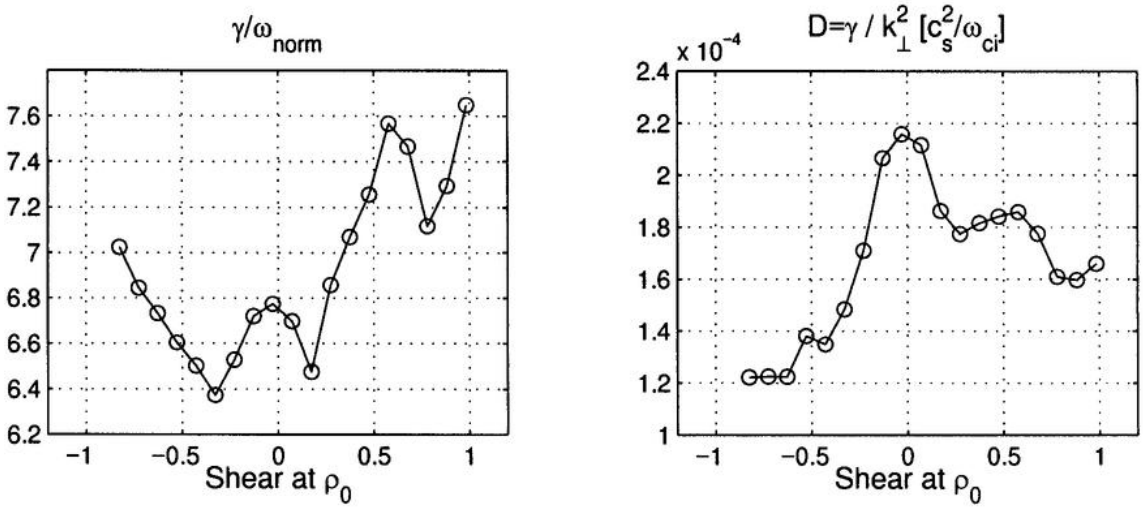

Figure 2.4: Effect of negative magnetic shear.

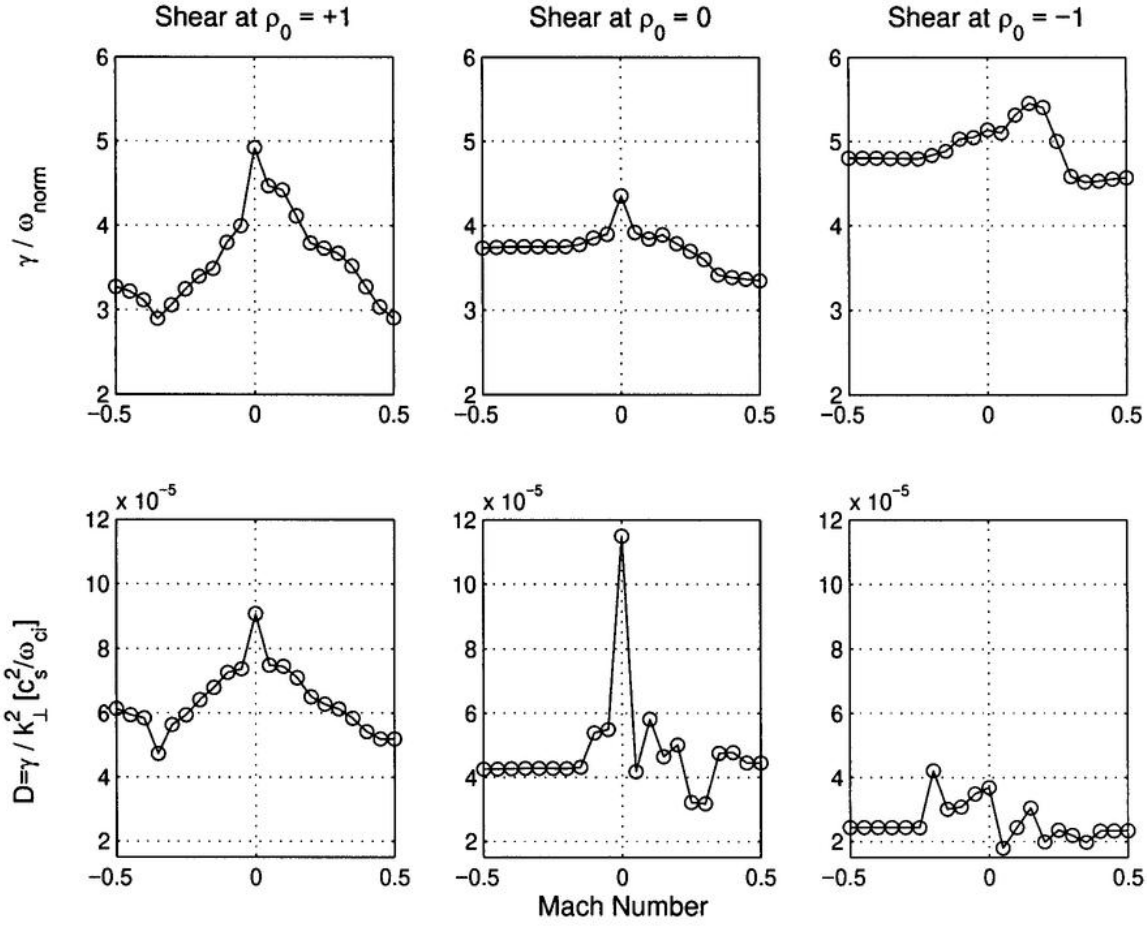

Figure 2.5: Magnetic shear and flow combined.

$\{+1,0,-1\}$ of the magnetic shear at the spot ρ_0 where the mode amplitude is the largest; Mach number is varied from -0.5 to 0.5. The second line shows the linear estimate for transport D for the same parameters. As seen in the first line, the effect of poloidal flow is greater for the positive value of magnetic shear. The second line shows that the combination of flow and negative magnetic shear reduces by about a factor four the linear estimate for transport, compared to the most unfavorable case (i.e. shearless without flow). It should be stressed that, as already explained, most of the points in Fig.2.5 represent slab modes and not toroidal modes. This should be kept in mind for later, when we will present the results of the kinetic code.

2.4 Conclusion

We are now done with the fluid model. Let us summarize what we wrote. A global fluid model has been coded in order to study effects of poloidal $E \times B$ flows as well as negative magnetic shear. The main drawback of the fluid model is that it exhibits plenty of slab-like modes, which are not strongly affected by poloidal flows. Therefore results show that poloidal flow has an important effect on ITG, but do not demonstrate complete stabilization. Moreover, negative magnetic shear does not present a systematic effect on stabilization. Nevertheless, a substantial reduction of mixing length estimate for transport has been observed.

It is important, in our opinion, to use a global model for the study of flow, because, as we have seen, flow shows no effect on the growth rate in a local dispersion relation and as shown by Taylor et al. [20], it cannot be thoroughly studied within a ballooning representation.

Time now to move to the more exciting kinetic model.

Chapter 3

Gyrokinetic Model

The simple way to go beyond the limitations of the fluid model was the use of a gyrokinetic model. The plasma is modeled by gyrokinetic ions with full FLR effects and adiabatic electrons. We linearize the gyrokinetic equation for ions, including a strong equilibrium electric field. Then the quasi-neutrality approximation is used to couple the ions to the electrons, which are considered adiabatic. This results in an eigenvalue integral equation for the ITG modes with strong electric fields. The spectral problem is solved in the full two-dimensional poloidal plane for a large aspect ratio tokamak.

3.1 General geometry

The first step is to include strong electric fields in the gyrokinetic formalism. This was done by Hahm [29] with the use of Hamiltonian mechanics in non-canonical variables and Lie transform formalism. We solve this new gyrokinetic equation using a perturbation method, as we are interested in the linear stability problem.

In [29], Hahm used the variables $\{\mathbf{R}, \alpha, \mu, v_{\|}, t\}$, being the guiding center position, Larmor rotation angle, magnetic moment, parallel velocity and time, respectively. But to simplify our linear calculations, we have decided to work with an "energy" variable ε instead of the parallel velocity $v_{\|}$, because, as we will see later, at the

lowest order in perturbation, it is a constant. We define it as:

$$\varepsilon := e\phi_0 + m\mu B + \frac{m}{2}\left(v_{\|}^2 + \mathbf{u}^2\right) \tag{3.1}$$

where e and m are the ion charge and mass respectively, ϕ_0 is the potential for the strong electric field, B is the modulus of the magnetic field, $\mathbf{u}$ is the sheared $E \times B$ flow:

$$\mathbf{u} := \frac{1}{B^2}\mathbf{B} \times \nabla\phi_0 \tag{3.2}$$

The second step is to apply an electrostatic perturbation $< \delta\phi >$ to the equilibrium plasma; the notation $< \cdots >$ represents an averaging over α, which appears via the Lie transform formalism. Given this, it is easily shown that:

$$\dot{\varepsilon} = -e\dot{\mathbf{R}} \cdot \nabla \left[< \delta\phi > (\mathbf{R}, \mu, t)\right] \tag{3.3}$$

where $\nabla = \partial_{\mathbf{R}}$ and we have [29]:

$$\dot{\mathbf{R}} = v_{\|}\mathbf{e}_{\|} + \mathbf{u} + \frac{1}{eB_{\|}^{\star}}\left[m\mu\nabla B + m\left(v_{\|}\mathbf{e}_{\|} + \mathbf{u}\right)\nabla\left(v_{\|}\mathbf{e}_{\|} + \mathbf{u}\right)\right] \tag{3.4}$$

where $B_{\|}^{\star} = B + (m/e)\mathbf{e}_{\|} \cdot \mathrm{rot}(v_{\|}\mathbf{e}_{\|} + \mathbf{u})$ and $\mathbf{e}_{\|} = \mathbf{B}/B$. It is possible to show, using the Lie transform formalism, that:

$$n_{ions}(\mathbf{x}, t) = \int B_{\|}^{\star}\left[F + \frac{e}{mB}\delta\tilde{\phi}\partial_{\mu}F + f\right] \cdot \delta(\mathbf{R} + \rho_L - \mathbf{x}) d\mathbf{R} d\alpha d\mu dv_{\|} \tag{3.5}$$

where $\mathbf{x}$ is the position of the particle and not the position of the guiding centers and with the following definitions: $\delta\tilde{\phi} = \delta\phi - < \delta\phi >$ and $\delta(\cdots)$ is the Dirac distribution.

With the $\{\mathbf{R}, \alpha, \mu, \varepsilon, t\}$ variables, the linearized gyrokinetic equation reads:

$$\partial_t f + \dot{\mathbf{R}} \cdot \nabla f = -\left[\frac{1}{B^2}\left(\mathbf{B} \times \nabla < \delta\phi >\right) \cdot \nabla F + \dot{\varepsilon}\partial_{\varepsilon}F\right] \tag{3.6}$$

where f is the first order perturbation part of the distribution function and F is the equilibrium part. We choose F to be a Maxwellian.

Eq.(3.6) can be formally solved by integrating over time along the equilibrium trajectories. To simplify the expressions, we first single out the adiabatic part of f, by defining the function g:

$$g := f - e < \delta\phi > \partial_{\varepsilon}F \tag{3.7}$$

which is the non-adiabatic part of the first order perturbation of the distribution function. We also use the fact that it is possible to write the electrostatic perturbation $< \delta\phi >$ as [10]:

$$< \delta\phi > (\mathbf{R}, \mu, t) = \exp(-i\omega t) \int_{\mathbb{R}^3} d\mathbf{k} \left[J_0(k_\perp \rho_L) \delta\hat{\phi}(\mathbf{k}) \exp(i\mathbf{k} \cdot \mathbf{R}) \right] \tag{3.8}$$

with $\omega \in \mathbb{C}$ representing the spectral approach and where $\delta\hat{\phi}(\mathbf{k})$ is the Fourier transform of the potential $\delta\phi(\mathbf{R}, \alpha, \mu)$, i.e. the electrostatic perturbation not averaged over α. The averaging over α is represented in the Bessel function.

Then the formal solution of Eq.(3.6) is:

$$g = -\frac{eF}{T_i} \int_{\mathbb{R}^3} d\mathbf{k} \left[J_0(k_\perp \rho_L) \exp\left(i\mathbf{k} \cdot \mathbf{R}(t) - i\omega t\right) (\omega - \omega^\star)\, i\mathcal{P} \cdot \delta\hat{\phi}(\mathbf{k}) \right] \tag{3.9}$$

where T_i is the ion equilibrium temperature, J_0 is the Bessel function, $k_\perp$ the component of $\mathbf{k}$ which is perpendicular to the magnetic field, ρ_L is the ion Larmor radius and we have defined the following differential operator:

$$\omega^\star := -\frac{iT_i}{eB} \left[\mathbf{e}_n \cdot \nabla \left(\ln F\right)\right] \left[\mathbf{e}_b \cdot \nabla\right] \tag{3.10}$$

where $\mathbf{e}_n$ and $\mathbf{e}_b$ are the normal and binormal unit vectors respectively, defined with respect to the flux surfaces and the field lines of the magnetic field.

The propagator $\mathcal{P}$ is defined as [10]:

$$\begin{aligned} \mathcal{P}(\mathbf{R}, \mathbf{k}, \varepsilon, \omega) &:= \int_{-\infty}^{t} dt' \exp\left[i\mathbf{k} \cdot (\mathbf{R}(t') - \mathbf{R}(t)) - i\omega\,(t' - t)\right] \\ &= \int_{-\infty}^{t} dt' \exp\left[i \int_{t}^{t'} \left(\mathbf{k} \cdot \dot{\mathbf{R}}(t'') - \omega\right) dt'' \right] \end{aligned} \tag{3.11}$$

At this point, we have a formal solution to the perturbation calculation. It is worth noting that this formal solution is nowhere explicitly modified by the strong electric fields. In fact, this solution is exactly the same as the one obtained by Brunner et al. [10]. The only effect of the strong electric field is to modify the equations of motion of the guiding centers, thus modifying the trajectories, which explicitly appear in Eq.(3.11). Thus, all the details of the numerical resolution of the problem will be the same as in [10]. We only need to compute an explicit formula for the propagator with strong electric fields.

3.2 Large aspect ratio tokamak

We have restricted ourselves to the case of a large aspect ratio tokamak, with circular concentric flux surfaces. The magnetic field is taken as:

$$\mathbf{B}(\rho,\theta) = B_0 \frac{R_0}{r(\rho)} \left(\mathbf{e}_\varphi + \frac{\rho}{R_0 q_s(\rho)} \mathbf{e}_\theta \right) \tag{3.12}$$

where R_0 is the major radius, $r(\rho) = R_0 + \rho\cos(\theta)$ is the cylindrical radius, B_0 is the magnetic field on the axis, $\mathbf{e}_\varphi$ is the unit vector along the toroidal angle, $\rho \in [0, a]$ is the minor radius, θ is the geometric poloidal angle, $q_s(\rho)$ is the safety factor, which is chosen arbitrarily, and $\mathbf{e}_\theta$ is the unit vector along the poloidal angle. We assume that $a/R_0 \ll 1$.

The last step before the explicit computation of the propagator, is the determination of the equilibrium trajectories of the guiding centers, i.e. the computation of $\mathbf{R}(t')$. To solve the equations of motion, we use an iterative method, considering that the drifts are a correction to the unperturbed trajectories. In this geometry, the equilibrium equations of motion for the guiding centers read [Eqs.(3.4) and (3.12)]:

$$\begin{aligned} \dot{\rho} &= -v_D \sin\theta + \frac{u^2(\rho)}{R_0\omega_{ci}} \sin\theta \\ \dot{\theta} &= \tilde{\omega}_t - \frac{v_D}{\rho}\cos\theta - \frac{u^2(\rho)}{\rho^2\omega_{ci}} \\ \dot{\varphi} &= \omega_t q_s(\rho) \end{aligned} \tag{3.13}$$

where $\omega_t := v_\parallel / R_0 q_s(\rho)$ is the poloidal transit frequency and $\tilde{\omega}_t := \omega_t + u(\rho)/\rho$, ω_{ci} is the ion cyclotron frequency, $\{\rho, \theta, \varphi\}$ are the toroidal variables, and v_D is the magnetic drift:

$$v_D = \frac{1}{R_0\omega_{ci}} \left(B_0\mu + {v_\parallel}^2 \right) \tag{3.14}$$

and $u(\rho)$ is obtained through (3.2) and (3.12):

$$\mathbf{u} = u(\rho) \left[1 + \frac{\rho}{R_0}\cos\theta \right] \mathbf{e}_\theta \tag{3.15}$$

From now on we will only consider highly passing ions and in order to solve the equations of motion, we will make the assumption that the parallel velocity is

constant: $v_{\|}(t) = v_{\|}(t_0)\ \forall t$. Solving iteratively Eqs.(3.13) yields:

$$\begin{aligned}
\rho(t') - \rho(t) &= \frac{1}{\tilde{\omega}_t}\left(v_D - \frac{u^2}{R_0\omega_{ci}}\right)\left[\cos(\tilde{\omega}_t t') - \cos(\tilde{\omega}_t t)\right] \\
\theta(t') - \theta(t) &= \tilde{\omega}_t(t'-t) - \frac{u^2}{R_0\omega_{ci}}(t'-t) - \frac{v_D}{\rho\tilde{\omega}_t}\left[\sin(\tilde{\omega}_t t') - \sin(\tilde{\omega}_t t)\right] \\
\varphi(t') - \varphi(t) &= \omega_t q_s (t'-t)
\end{aligned} \tag{3.16}$$

These equations are what we were seeking: we can now safely proceed to the explicit computation of the propagator.

Before going further, we would like to point out that we have in fact used a toroidal wave decomposition rather than the standard plane wave representation. Thus, Eq.(3.8) should read:

$$\int_{\mathbb{R}^3} d\mathbf{k}\left[\delta\hat{\phi}(\mathbf{k})\exp(i\mathbf{k}\cdot\mathbf{R})\right] = \sum_{k,m\in\mathbb{Z}} \delta\hat{\phi}_{(k,m)}\exp\left[i\left(k\frac{2\pi}{\Delta\rho}\right)\rho + im\theta + in\varphi\right] \tag{3.17}$$

where $\Delta\rho = (\rho_{Max} - \rho_{min})$ and $[\rho_{min}, \rho_{Max}]$ are the boundary within which we solve the problem. m and n are the poloidal and toroidal wave numbers, respectively, and $n \in \mathbb{Z}$ is fixed because the problem is axisymmetric. This decomposition implies an approximation on the geometry, which implications are fully discussed in [9].

Therefore, using Eq.(3.11), the iterative integration of the guiding centers trajectories and (3.17), it can be shown that the propagator becomes:

$$\mathcal{P}(\theta) = \sum_{p,p'\in\mathbb{Z}} J_p(x)J_{p'}(x)\frac{\exp\left[i(p-p')(\theta+\bar{\theta})\right]}{i\left(y - \omega + p\tilde{\omega}_t\right)} \tag{3.18}$$

where J_p are the Bessel functions and we have used the following definitions:

$$\begin{aligned}
x &= \left[\left(k\frac{2\pi}{\Delta\rho}\right)^2\frac{1}{\tilde{\omega}_t^2}\left(v_D - \frac{u^2}{R_0\omega_{ci}}\right)^2 + \left(\frac{mv_D}{\rho\tilde{\omega}_t}\right)^2\right]^{\frac{1}{2}} \\
y &= m\tilde{\omega}_t + nq_s\omega_t - m\frac{u^2}{\rho^2\omega_{ci}} = k_{\|}v_{\|} + m\frac{u}{\rho}\left(1 - \frac{u}{\rho\omega_{ci}}\right) \\
\cos\bar{\theta} &= \left(k\frac{2\pi}{\Delta\rho}\right)\frac{1}{\tilde{\omega}_t}\left(v_D - \frac{u^2}{R_0\omega_{ci}}\right)/x \\
\sin\bar{\theta} &= \left(\frac{mv_D}{\rho\tilde{\omega}_t}\right)/x
\end{aligned} \tag{3.19}$$

where $k_{\|} := (m + nq_s)/(R_0 q_s)$. Eq.(3.18) is all we needed: it is the expression of the propagator in presence of a strong electric field. The set of equations is now complete: using (3.5), (3.7), (3.9), (3.18), the quasi-neutrality approximation and the adiabatic electrons, we can produce an eigenvalue integral equation which considers the full 2-D poloidal plane. It can be solved to determine the spectrum of the ITG modes in the framework of gyrokinetic theory. The details are to be found in [10].

3.3 Trapped Ions

In the previous formulation, we assumed that the parallel velocity was a constant, which has been shown [10] to be a very good approximation for passing ions. In this section we will develop the model a bit further in order to allow for trapped ions. Previous equations remain valid up to Eq.(3.15) included. Again, we will use exactly the same steps made in [10], having basically only to add a change of variables.

Let us start with the equations of motion of the equilibrium. Removing the drifts from Eq.(3.13), we get:

$$\begin{aligned} \dot{\rho} &= 0 \\ \dot{\theta} &= v_{\|}/R_0 q_s(\rho) + u(\rho)/\rho \\ \dot{\varphi} &= v_{\|}/R_0 \end{aligned} \tag{3.20}$$

The question now is how to model the evolution of $v_{\|}$. As is shown in Hahm's paper [29], the time evolution of $v_{\|}$ is given by:

$$\dot{v_{\|}} = -\mu \mathbf{e}_{\|} \cdot \nabla_{\|} B + \mathbf{u}\left(\mathbf{e}_{\|} \times \mathrm{rot}\left(v_{\|}\mathbf{e}_{\|} + \mathbf{u}\right)\right) \tag{3.21}$$

This expression is already simplified, as we have not written the terms that vanish due to the following: $\{\phi_0, \mathbf{u}^2\}$ are only functions of ρ and the operator $\mathbf{e}_{\|} \cdot \nabla_{\|}$ does only produce derivatives in $\{\varphi, \theta\}$.

We will now show that the second term in the right handside of Eq.(3.21) can be neglected. Using Eq.(3.12), it is easy to show that:

$$\begin{aligned} -\mu \mathbf{e}_{\|} \cdot \nabla_{\|} B &\approx -\left(\frac{\rho}{R_0 q_s(\rho)}\right)\left(\frac{v_{thi}^2}{R_0}\right)\sin\theta \\ +\mathbf{u}\left(\mathbf{e}_{\|} \times \mathrm{rot}\left(v_{\|}\mathbf{e}_{\|} + \mathbf{u}\right)\right) &\approx -\mathrm{Mach}\left(\frac{v_{thi}^2}{R_0}\right)\sin\theta \end{aligned} \tag{3.22}$$

where we have used the following normalization: $u(\rho) \approx \mathrm{Mach} \cdot v_{thi}$. Eq.(3.22) clearly shows that that as long as:

$$\mathrm{Mach} \ll \rho / R_0 q_s \tag{3.23}$$

we can neglect the second term in the right handside of Eq.(3.21). Therefore, we simply will consider the following equation for the parallel velocity:

$$\dot{v_{\|}} = -\mu \mathbf{e}_{\|} \cdot \nabla_{\|} B \tag{3.24}$$

The idea now is to simplify Eq.(3.20) with a change of variables. Trying to recover what we had without flow, we chose to use:

$$v'_{\|} = v_{\|} + \frac{u(\rho)}{\rho} \cdot q_s(\rho) \cdot R_0 \tag{3.25}$$

which leads to the following equations:

$$\begin{aligned} \dot{v}'_{\|} &= \dot{v}_{\|} \\ \dot{\theta} &= v'_{\|} / R_0 q_s(\rho) \\ W'(t) &= \frac{1}{2} {v'_{\|}}^2 + \mu B = W'(t_o) \quad \forall t \end{aligned} \tag{3.26}$$

where $W'(t)$ is an integral of motion and we can call it the *energy*. It is easy to prove that $\dot{W}'(t) = 0$. We have thus obtained equations of motion that are exactly like the ones without flow, but in the new variable $v'_{\|}$. Therefore we can derive equivalents to all the formulas first obtained by Brunner et al. [10]. Let us go through some of the most important.

First of all, the distinction between trapped and passing ions is summarized by the following quantity:

$$\chi^2 = \frac{W' - \mu B_0 \left(1 - \rho / R_0\right)}{2 \mu B_0 \rho / R_0} \tag{3.27}$$

and when $\chi^2 > 1$ we are dealing with passing particles, while with $\chi^2 \leq 1$ we are considering trapped ions.

Second, we can compute the fraction of particles which are trapped and passing: this fraction will be a function of the Mach number, as could have been expected. The fraction of trapped ions α_t is thus:

$$\begin{aligned} \alpha_t(u) &:= \int_{\Omega_t} F(\mathbf{v}) d\mathbf{v} \\ &= \alpha_0 \cdot \exp\left[-(u \cdot q_s \cdot R_0/\rho)^2/2T_i\right] \end{aligned} \tag{3.28}$$

where Ω_t represents the domain of only trapped ions and α_0 is the fraction of trapped particles without flow. We see that an increasing flow, whatever its sign, will decrease the number of trapped particles. But this effect remains small within the approximation (3.23).

Now, we would like to say a word about the invariant p_φ. As tokamaks are axisymmetric, the variable φ is therefore cyclic and its associated component in the fundamental form of Hamiltonian mechanics must be a constant [33]. In our case [29], this simply gives:

$$p_\varphi(t) := \rho + v_{||} \frac{R_0 q_s(\rho)}{\rho w_{ci}} = p_\varphi(t_0) \quad \forall t \tag{3.29}$$

and we have the expression for the invariant with $E \times B$ flows.

The only remaining modification to be done is in the precessional drift. Indeed, for the equations of motion, we did exactly like Brunner [10], assuming that all trapped ions are deeply trapped, which allows to solve iteratively the equations of motion in the new parallel velocity. Let us now have a look at the precessional drift. Taking the equations of motion in the old variable $v_{||}$ (3.20), we can compute the precessional drift $\tau < \dot{\varphi} >$, where τ is the poloidal revolution period (banana period). The algebra is in no way new and pretty long, with the apparition of the complete elliptic integrals along the way, so we present the final result only:

$$\tau < \dot{\varphi} > = [\tau < \dot{\varphi} >]_{N.F.} - \tau \left(\frac{u(\rho) q_s(\rho)}{\rho} \right) + O\left[u(\rho)^2\right] \tag{3.30}$$

where $[\tau < \dot{\varphi} >]_{N.F.}$ stands for the precessional drift with No Flow and we will not consider the $O[u(\rho)^2]$, due to the condition (3.23). This is it, we now have a complete model for trapped ions with $E \times B$ flows. The only differences with respect to Brunner's work [10] are Eqs.(3.28) and (3.30).

3.4 Numerical Implementation

To give a resume, we have solved the linearized gyrokinetic equation for ions, in a spectral approach. This solution coupled with the adiabatic electrons gives rise to an integral equation for the eigenmodes of the electrostatic potential. The free input data parameters for our problem are: the profiles of equilibrium quantities, the parameters of the equilibrium geometry, the toroidal wave number n, and the profile of the $E \times B$ sheared poloidal flow u. Given these, the task is to find the eigenmodes of the plasma, i.e. find the values of ω for which there is a non-trivial solution $\delta\hat{\phi}$ to the integral equation.

We will not discuss in details the numerical approach, because it is rigorously the same as the one used by Brunner [10]. Indeed, we did not start from scratch, but had simply to modify the already existing and extensively benchmarked [30] Brunner's code: GLOGYSTO. The modifications we had to include did not request a modification of any of the numerical tools used. To put it simply, they only changed the function we had to integrate. The main modification comes from a symmetry breaking, that occurs in the integration over $v_{||}$, due to the flow. Indeed, the original formulation did an explicit use of the $v_{||} \to -v_{||}$ symmetry in the precalculation part [10]. We therefore had to, roughly speaking, double the memory use. Altogether, doing things properly, this did not result in a problem.

It must also be stressed that Brunner's code includes the possibility to study both adiabatic and trapped electrons, with a bounce averaged equation for the trapped ones. This part did not change, because we did not consider the effect of $E \times B$ flows on electrons, as it is smaller than the one on ions by a mass ratio factor. Therefore,

although we did not present the equation, we have the possibility to include trapped electrons in our system [10].

Nevertheless, for those not acquainted with Brunner's work, we give here a brief account of the numerical methods. As noted in Eq.(3.17), the two space dimensions are decomposed on the Fourier functions basis. For the determination of the significant Fourier components to include in the computation, one should read Brunner, but the main argument remains naturally the convergence. The radial integration is performed on an equidistant mesh using the FFT algorithm. The velocity integrals are not performed on the whole $\mathbb{R}^3$, but reduced to a sphere of radius $n \cdot v_{thi}$ where $n \in \mathbb{N} \approx 5$. The extended trapezoidal rule is used for this integration.

At this point, there are two questions that need to be answered. Does the inclusion of $E \times B$ flows deteriorate the numerical convergence ? Are the observed effects

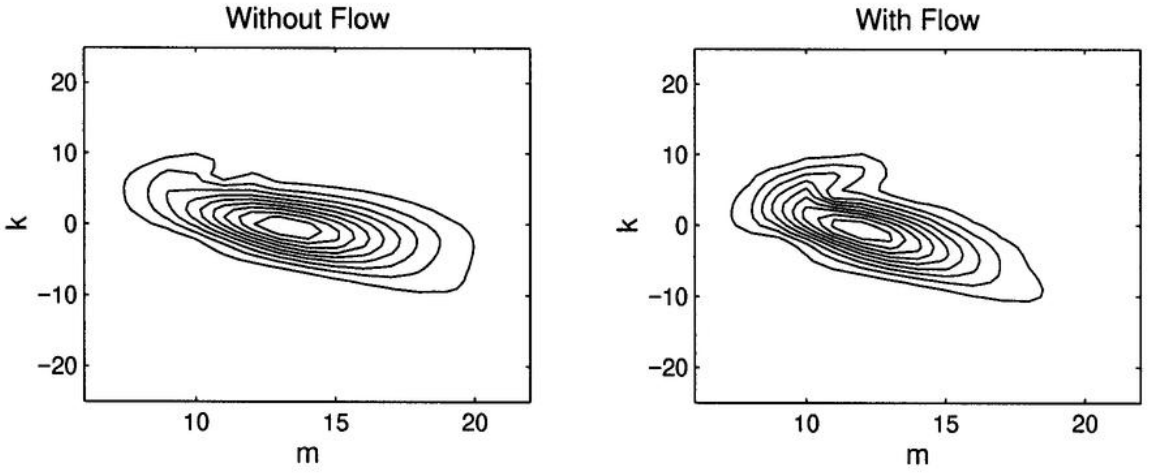

Figure 3.1: No strong modification of the mode in the Fourier space when $E \times B$ flows are included. This case corresponds to a very strong physical effect: a stabilization by a factor three.

of $E \times B$ flows physical or numerical ? This last question is answered extensively in Chapter 4: Gyrokinetic Results, where we do a benchmark between our spectral code and a PIC code, which is a completely different numerical approach. As discussed later on in more details, the effect of $E \times B$ flows are the same in the spectral and PIC codes, therefore we can trust our model. The answer to the first question

can convincingly be met by the Fig.3.1, in which we see an eigenmode in the Fourier space. As the figure demonstrate, inclusion of $E \times B$ flow does not affect much the extent of the Fourier space required. Nevertheless, the presented inclusion of flow has a very strong stabilizing effect (factor three) and a large Doppler shift of the frequency.

There are two methods to find the eigenvalues in the complex plane. In fact, our problem, after discretization, can be written like this:

$$\sum_j M_{ij}(\omega) \cdot \delta\hat{\phi}_j = 0 \tag{3.31}$$

Therefore, our task is simply to find the zeros of the analytical function $f(\omega) := \det(M)$. This is done using two different methods, depending on the number of eigenvalues present in a region of the complex plane $\mathbb{C}$. If the number of zeros is small, typically less than three, there is a very fast and efficient method based on the Nyquist theorem [9], [31]. It usually requires the sampling of f on eight to twenty points on a Jordan curve enclosing the eigenvalues. Otherwise, we need to do a rectangular scan of $\mathbb{C}$, and then plot the contour lines for $\Re(f) = 0$ and $\Im(f) = 0$: the intersections of these contour lines are our eigenvalues. This method requires normally a sampling of f on a mesh of $25 \times 25 = 625$ points. As we see, there is more than an order of magnitude difference between the two methods, but one cannot always avoid using the scan.

Let us now say a word about the computer implementation. The GLOGYSTO code, originally written in Fortran 77, has been upgraded to Fortran 90 for the author convenience and the sake of portability. NAG routines are used for the FFT routines and most of the special functions, while LAPACK routines are used for the matrix calculations. The code was used on the following platforms successfully: on the Silicon Graphics R10000 processor, on the Sun Microsystems Sparc Ultra-2 processor and on the Cray J90 supercomputer processor. There exists also a parallel version of the code, but most of the runs were performed using the single processor

version due to a surcharge of the EPFL parallel machine.

Chapter 4

Gyrokinetic Results

Now that we have formulated the equations and coded them, there are several interesting studies that we can perform. This chapter will present the following studies:

- effect of different profiles of $E \times B$
- effect of $E \times B$ flows in combination with magnetic shear
- experimental comparison with the Asdex Upgrade tokamak

We would like also to point out that, although we did include the analytical calculations for the study of Trapped Ion Modes under the effect of $E \times B$ flows in this PhD, we did not have the time to run any case with TIM modes.

4.1 Various Profiles of $E \times B$ flows

In this section we will study how various profiles of $E \times B$ poloidal flows affect the ITG toroidal modes. To make it short, we will see that the shear of the poloidal rotation velocity has a stabilizing effect, but in no way is this effect stronger than the one due to the value of the poloidal rotation velocity. We will also see that the value of the second derivative of the poloidal rotation velocity is an irrelevant quantity.

For this study, we chose the following parameters: $a = 0.21$[m], $R_0 = 1.19$[m], $B_0 = 1$[Tesla], $T_e = T_i = 1$[keV], the ions were hydrogen, $q_s \in [1, 5]$ and $q_s \approx 2$

where the mode amplitude is maximum. The parameters are set so that the ITG toroidal modes are much more unstable than the ITG slab-like modes that exist even in toroidal geometry. In this study we are only interested in ITG toroidal modes.

We have now to decide what value of n we want to study. It seems to us natural to be mainly interested in the most unstable n of our system. We have therefore made a scan in n in order to find the most unstable eigenmode, results being plotted

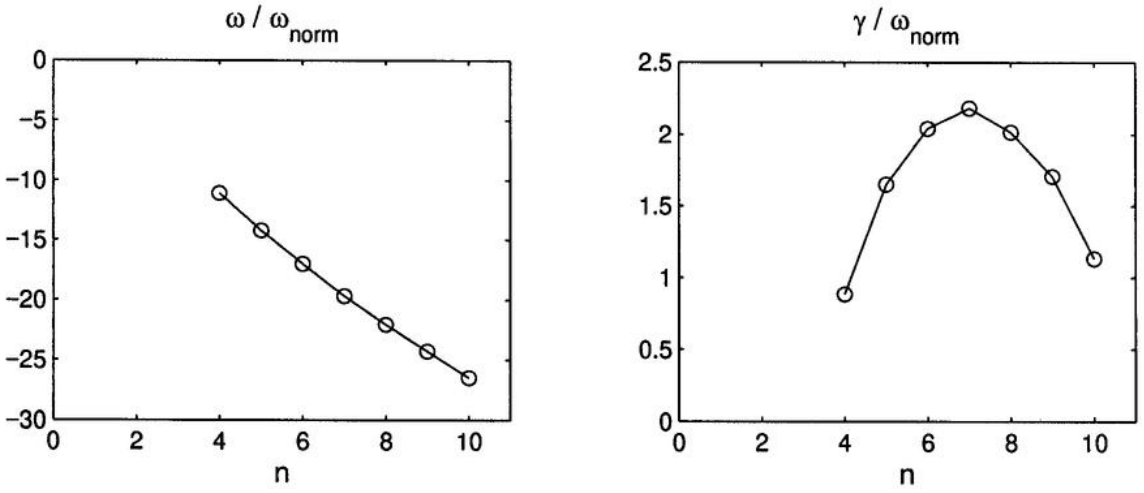

Figure 4.1: Scan in n to find the most unstable eigenmode of the system.

in Fig.4.1. Clearly, the most unstable mode is given by $n = 7$, thus we studied only this mode. This might look like an awkwardly low value of n, but it must be stressed that as our calculations are global, we can impose the value of ρ_L, but the value of $k_\perp$ is given by the results of the calculations and we know that the most unstable toroidal ITG mode will have $k_\perp \cdot \rho_L \approx 0.5$, thus the concept of "high n" is relative to the plasma studied.

Now we come to the choice of the $E \times B$ profile. As seen in Eq.(1.2) and in the definition of $\tilde{\omega}_t := \omega_t + u(\rho)/\rho$ (see Eq.(3.13)), the important quantity is $u(\rho)/\rho$. Therefore, here is how we chose the profile of $E \times B$ poloidal flow:

$$\frac{u(s)}{s} = \text{Mach} \cdot v_{thi} \left[u_0 + u_1 s + u_2 s^2\right] \tag{4.1}$$

where v_{thi} is the ion thermal velocity and $s = \rho/a$ is the normalized radial variable.

This allows us to study separately the effect of constant flow, constant shear of flow and non constant shear of flow.

It is well known that the radial profile of the ITG toroidal modes is determined by the logarithmic derivative of the ion temperature and the safety factor, the modes trying to maximize the drive of the temperature gradient, while minimizing their $k_{\|}$. It is also very well known that the ITG toroidal modes do balloon in the region of unfavorable magnetic curvature, that is around $\theta \approx 0$. From now on, we will use $\{s_o, \theta_o\}$ to name the normalized radius and poloidal angle where the mode amplitude is maximum.

We can now describe the shapes of $u(s)$ that we considered. There are three basic

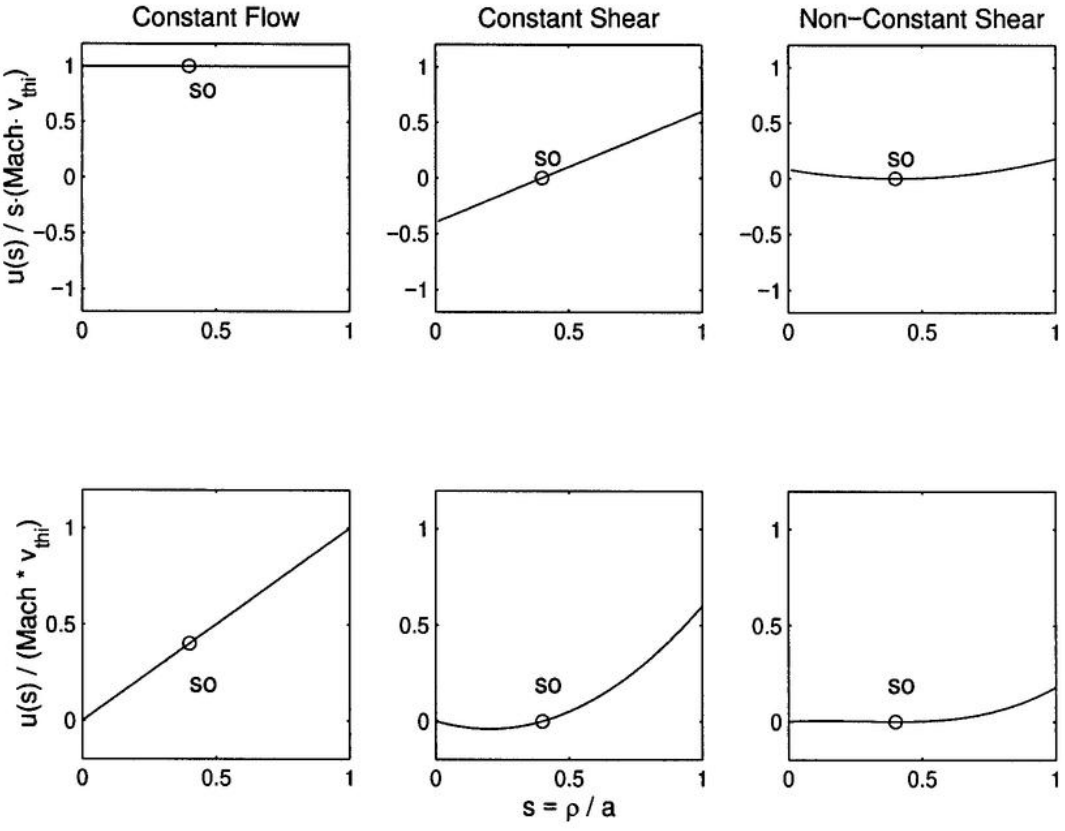

Figure 4.2: The three different shapes of $E \times B$ flow: $u(s)/s$ and $u(s)$

cases and they are chosen starting with the constant poloidal rotation velocity. We want $u(s)/s$ to be equal to 1 and therefore, we took: $u_0 = 1$, $u_1 = 0$, $u_2 = 0$. we will call this profile "constant flow". Then, we want to "normalize" the values of the first

and second derivatives, therefore we choose profiles such that $\partial_s(u(s)/s) = 1$ and $\partial_s^2(u(s)/s) = 1$ everywhere. Therefore, the second shape, that we will call "constant shear", is thus given by: $u_0 = -s_o$, $u_1 = 1$, $u_2 = 0$; the flow vanishes at s_o, but it has constant shear. And the third shape, that we will call "non constant shear", is given by: $u_0 = \frac{1}{2}s_o^2$, $u_1 = -s_o$, $u_2 = \frac{1}{2}$. The flow and its constant shear both vanish at s_o, but the profile being parabolic, the second derivative of flow is not vanishing there. The three profiles are plotted in Fig.4.2. For each of them, the "driving terms" (the value of $u(s)/s$, the first derivative of $u(s)/s$ and the second derivative of $u(s)/s$ respectively) have all the same value at s_o: Mach $\cdot\, v_{thi}$.

Let us first see the effect of the $E \times B$ flow on the frequency ω and growth rate γ of a toroidal ITG mode. Results are shown in Fig.4.3 and Fig.4.4 where we can compare the different profiles of flow. The evolution of the frequencies is easily understood: for the constant flow case, we see a simple Doppler shift of the frequency, while for the other two cases we see that the frequency is unaffected. This is normal, as for these two cases there is no effective value of flow at s_o. Let us now have a look at the growth rates. We clearly see that the most stabilizing effect is due to the constant flow profile, while the constant shear is also strongly stabilizing. On the other hand, the second derivative of flow is completely ineffective: it does not at all affect the mode. We will explain the mechanism that leads to the observed stabilizations, but we would first offer a validation of our results.

We have two validations for these results: a comparison with a local dispersion relation and a benchmark with a global PIC code (Fig.4.5). Let us begin with the local dispersion relation. A kinetic local dispersion relation has been derived by Brunner [10] for the study of the ITG modes without flow. The introduction of flow can simply be seen as a Doppler shift in the frequency, given by Mach $\cdot\, v_{thi} \cdot k_\theta \cdot u(s_o)$ Therefore, in cases where $u(s_o) = 0$, one expects no variation of the frequency and this is exactly what is observed for both the constant shear case and non-constant shear case. For the constant flow case, one expects a Doppler shift and one

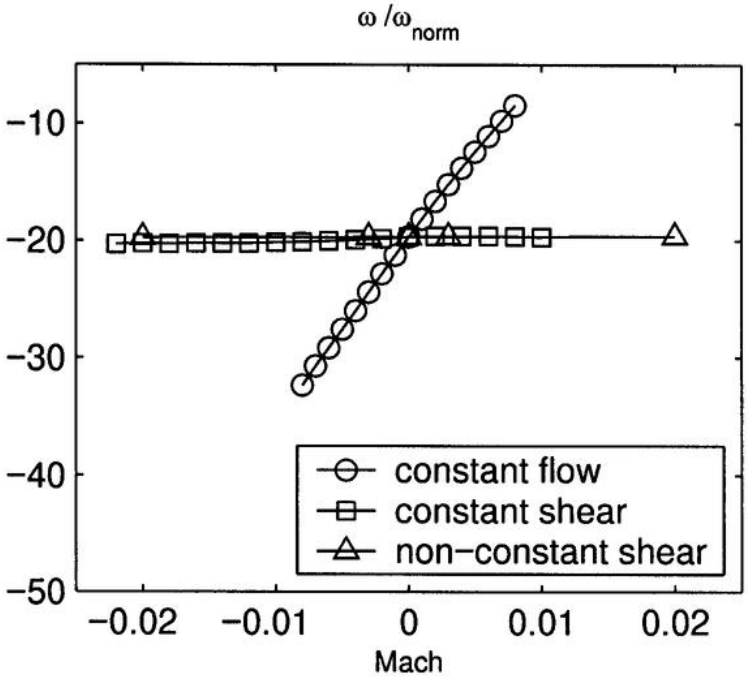

Figure 4.3: Frequency as a function of Mach number, $\omega_{norm} = v_{thi}^2/[\omega_{ci}a^2]$. The 'circles' stand for the 'constant flow', the 'squares' for the 'constant shear' and the 'triangles' for the 'non-constant shear'.

can compare the global spectral code with the dispersion relation. This is done in Fig.4.5. To have a benchmark for our growth rates, we did a comparison with a PIC code [32], modified by L. Villard to include $E \times B$ flows. The results of the PIC code are also shown in Fig.4.5. They are in excellent qualitative agreement with the results of the spectral code. The values of the frequencies are perfectly matching, while the values of the growth rates have a perfectly similar functional dependence on the Mach number, although the values are only in an agreement of 20%. This discrepancy does exist even for a vanishing Mach number and is simply explained by the different approximations used by both codes. For instance, the PIC code does not have an exact resolution of the linearized gyrokinetic equation to all orders in Larmor, while the spectral code does. For a detailed discussion of these issues see [30]. It is simply important to know that this discrepancy is not due to $E \times B$ flows. We can also add that we chose our physical parameters in order to have only a very unstable toroidal ITG mode and no slab-like or TIM modes, that is we

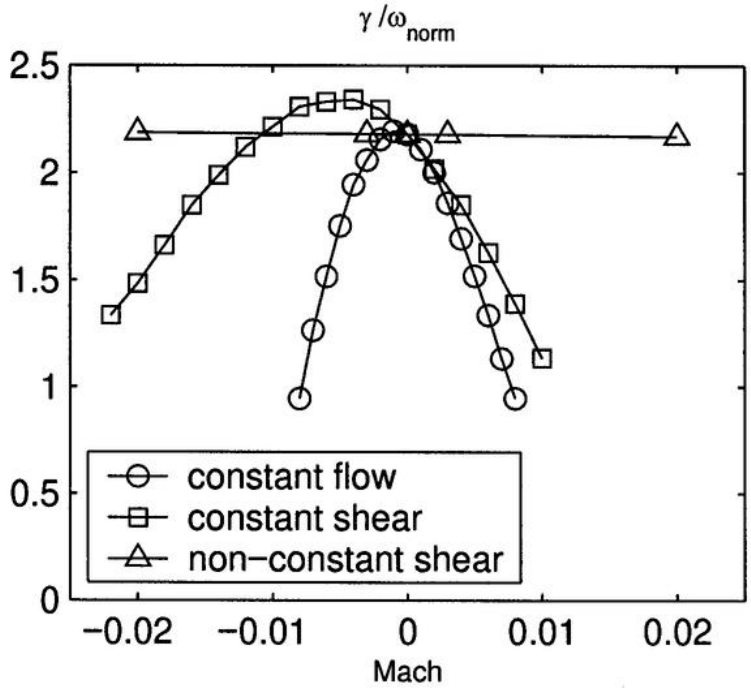

Figure 4.4: Growth rate as a function of Mach number. The 'circles' stand for the 'constant flow', the 'squares' for the 'constant shear and the 'triangles' for the 'non-constant shear'.

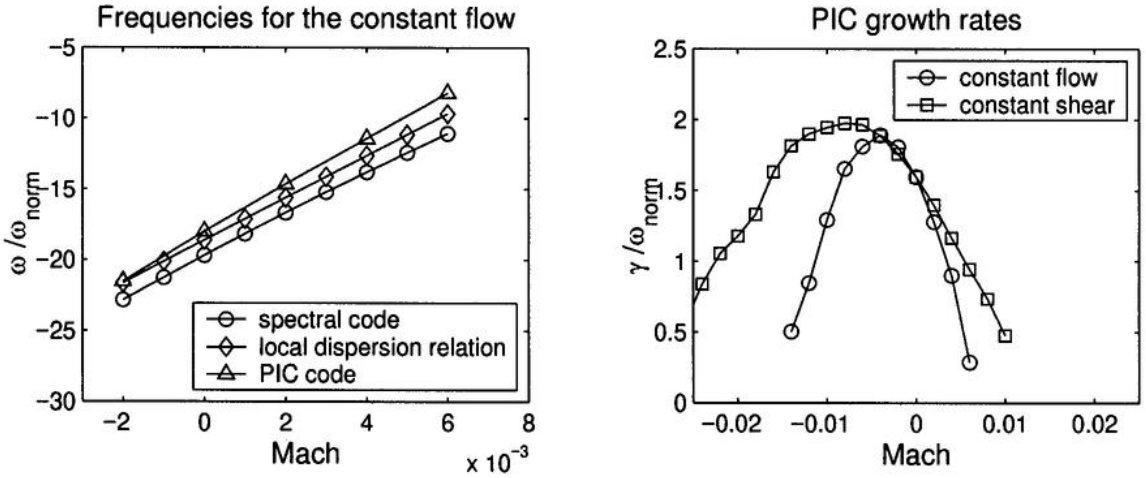

Figure 4.5: Benchmark with local dispersion relation and PIC code.

adjusted the parameters so to have $\omega_b \ll \omega$, where ω_b is the bounce frequency. The PIC code allowed a verification of that, as it includes both the passing and trapped ions dynamics. It showed that for this case, runs with and without trapped ions produced exactly the same modes.

One legitimate question is whether we are following one particular mode in our scans in Mach number or if we are checking the whole complex plane. To this question, it must be answered that checking the "whole" complex plane is by no means possible, but the comparison with the PIC code, which is only able to produce the most unstable ITG mode in the system, shows that there are no new unstable modes popping out. This is normal, as we chose our parameters so that there would be only a strongly unstable ITG toroidal mode, while there are some other modes, but much less unstable. Therefore in Fig.4.3 and Fig.4.4 it must be considered that we plot the evolution of the most unstable mode.

Now, we would like to discuss the mechanism of stabilization. In Fig.4.6 we show the effect of $E \times B$ flows on the poloidal contour plots of the electrostatic potential. The constant flow case is presented in the left column, while the constant shear case is in the right column. As one sees, there is not much qualitative difference between the two cases, the constant shear case needing simply a larger value of the Mach number. Before going further, it is important to stress that due to a convention in the code, a positive Mach number refers to plasma rotation in the clockwise direction.

Let us begin with the "constant flow" case: left column of Fig.4.6. It is obvious that the mode is simply rotated along with the plasma, that is the region θ_o where the mode balloons is moved. The consequence of which is to move the mode maximum amplitude region away from the unfavorable magnetic curvature region, reducing therefore the instability. A negative Mach number means a poloidal flow going upward on the external side of the plasma. Thus, for low negative values of Mach number, θ_o is first moved to a more unfavorable position, thus destabilizing the ITG. But, for stronger Mach number, θ_o moves further, leaving the unfavorable region, finally producing a strong stabilization of the toroidal ITG. This effect is naturally only effective for toroidal ITG modes, as the unfavorable magnetic curvature is for them necessary, while slab ITG modes can live without it.

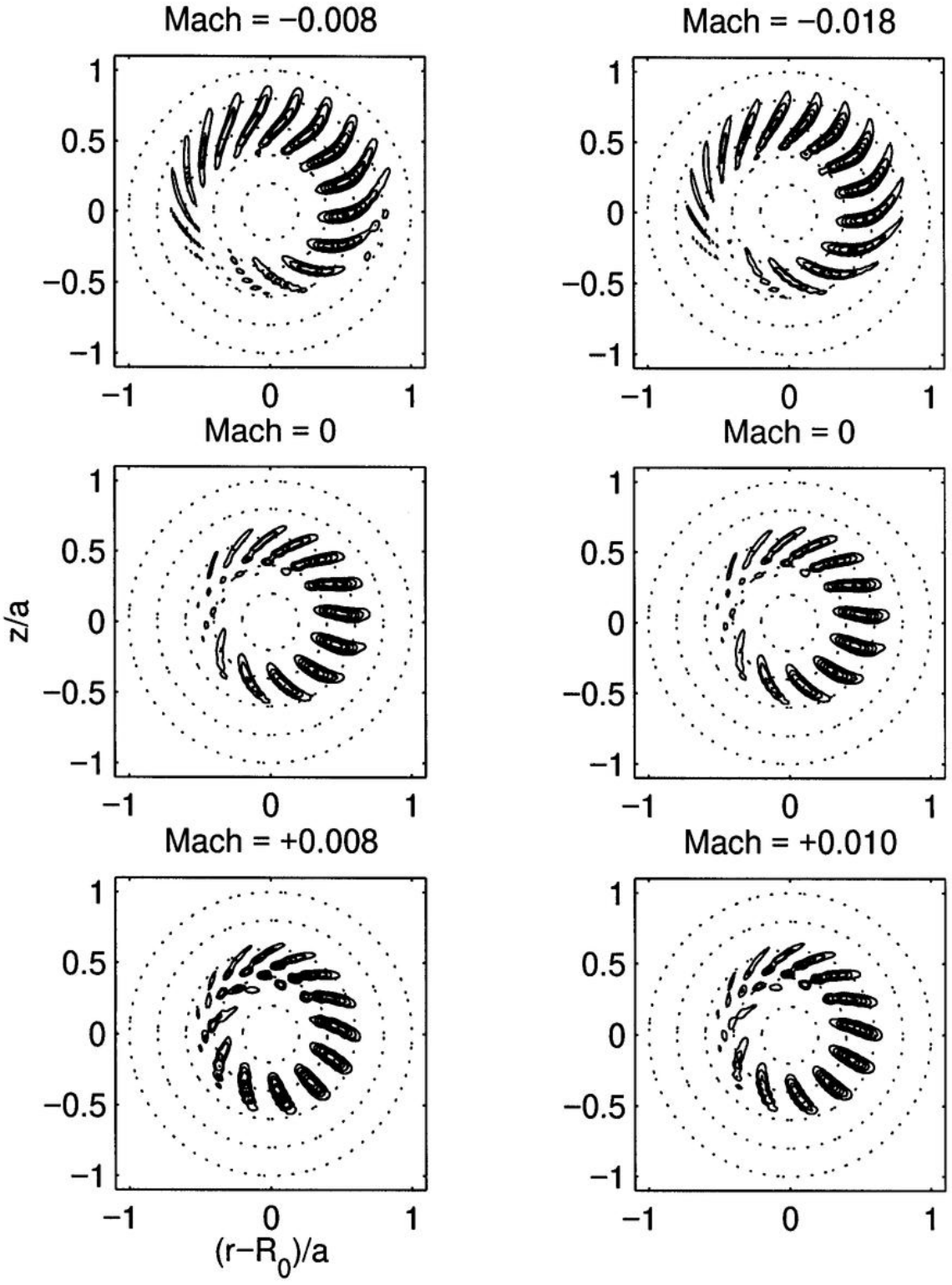

Figure 4.6: Contours of ITG mode in the poloidal plane for various Mach numbers. On the left is the Constant Flow case, while on the right is the Constant Shear case.

Now, let us have a look at he "constant shear" profile, that is the right column of Fig.4.6. It is difficult to see much difference with the "constant flow" case. It looks like if the mode, being global, had to choose between one of the sides of the flow and chose the external rotation, thus being affected like by the value of flow. The main difference being now that of course, the value of flow is not the same as before, resulting in different values of Mach numbers. It must be stressed that this result is in complete agreement with the observations of Kim and Kishimoto [27]: they also observed that a sheared poloidal $E \times B$ flow does affect the value of θ_o, therefore stabilizing the toroidal ITG mode. Indeed, the right column of Fig.4.6 looks very much alike their own figures. But they did not investigate the effect of a non-sheared $E \times B$ flow.

Now, coming back to Fig.4.4, we see that the "non constant shear" has clearly no relevant effect. This is in contradiction with most models, but assuming that our explanation of the mechanism of stabilization is correct (that is: the mode is stabilized because it is removed from the region of unfavorable magnetic curvature), then the non-effect of non-constant shear is obvious, as looking at Fig.4.2 clearly shows that the value of flow is almost zero everywhere for this case.

Now we would like to briefly describe the effect of the $E \times B$ flow on $k_\perp$, and $k_\parallel$ that we can estimate by averaging over the eigenmode: $k_\perp^2 = \langle \nabla_\perp \delta\phi^\star \cdot \nabla_\perp \delta\phi \rangle / \langle \delta\phi^* \delta\phi \rangle$ and $k_\parallel^2 = \langle \nabla_\parallel \delta\phi^\star \cdot \nabla_\parallel \delta\phi \rangle / \langle \delta\phi^* \delta\phi \rangle$. The results are plotted in Fig.4.7. We see that the variations of $k_\perp$ and $k_\parallel$ are exactly matching the variations of γ: when the mode gets stabilized, both $k_\perp$ and $k_\parallel$ are increasing and for the small region where the mode gets more unstable, both $k_\perp$ and $k_\parallel$ are decreasing. Although the absolute increase in $k_\perp$ is small, it nevertheless goes in the "good direction", that is it tends to reduce the linear estimate for the diffusion coefficient $D = \gamma / k_\perp^2$.

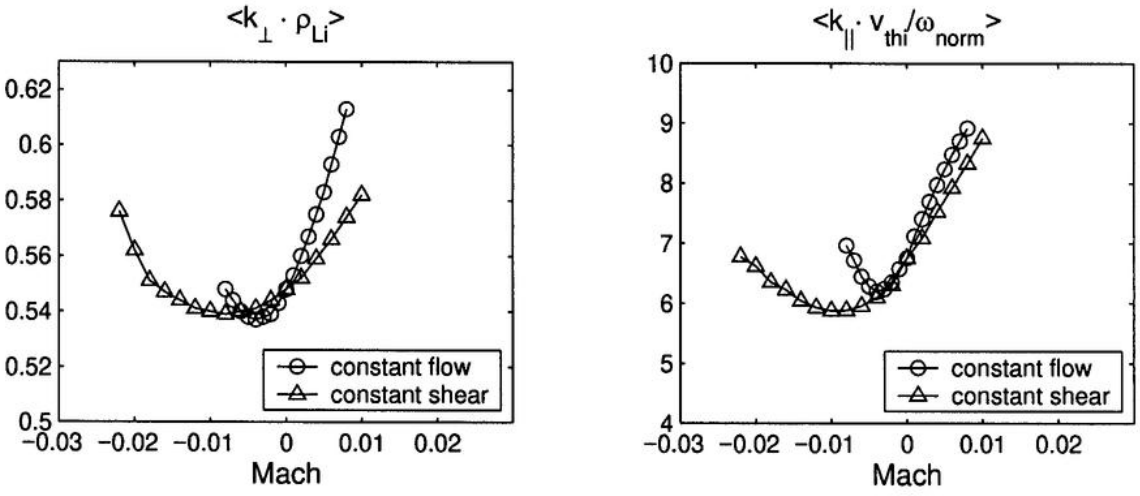

Figure 4.7: $k_\perp$ and $k_{||}$ as functions of Mach number. The 'circles' stand for the 'constant flow' and the 'triangles' for the 'constant shear'.

4.2 Various Magnetic Shears

It is often claimed that negative magnetic shear should be a main component of the ITB creation. Nevertheless, Brunner noticed [10] that with our model negative magnetic shear on its own does not exhibit a spectacular effect, but of course, that was done without $E \times B$ flows. Now the question arises, can $E \times B$ flows interact with a negative magnetic shear so as to produce a multiplicative effect ?

In order to answer this question, we have chosen the following physical system: $a = 0.5$[m], $R_0 = 2$[m], $B_0 = 1$[Tesla], $T_e = T_i = 2.13$[keV], the ions are hydrogen, $q_s(s_o) = 1.5$ and the most unstable mode is found for $n = 10$. Then, as we did in the fluid case, we have kept the value of $q_s(s_o)$ constant while changing the value of magnetic shear (simply called shear from now on) $(s_o \cdot d_s q_s(s_o))/q_s(s_o)$. We considered the following values for the shear: $\{-1, 0, +1\}$. This study, without $E \times B$ flows, had been already done by Brunner [10]. The qualitative nature of the modes changes for the three cases as is to be observed in Fig.4.8. The positive shear case clearly exhibits a toroidal nature, while the negative shear mode does not balloon and is therefore more of a slab nature. As expected, the vanishing shear case is somewhere in between the two other cases.

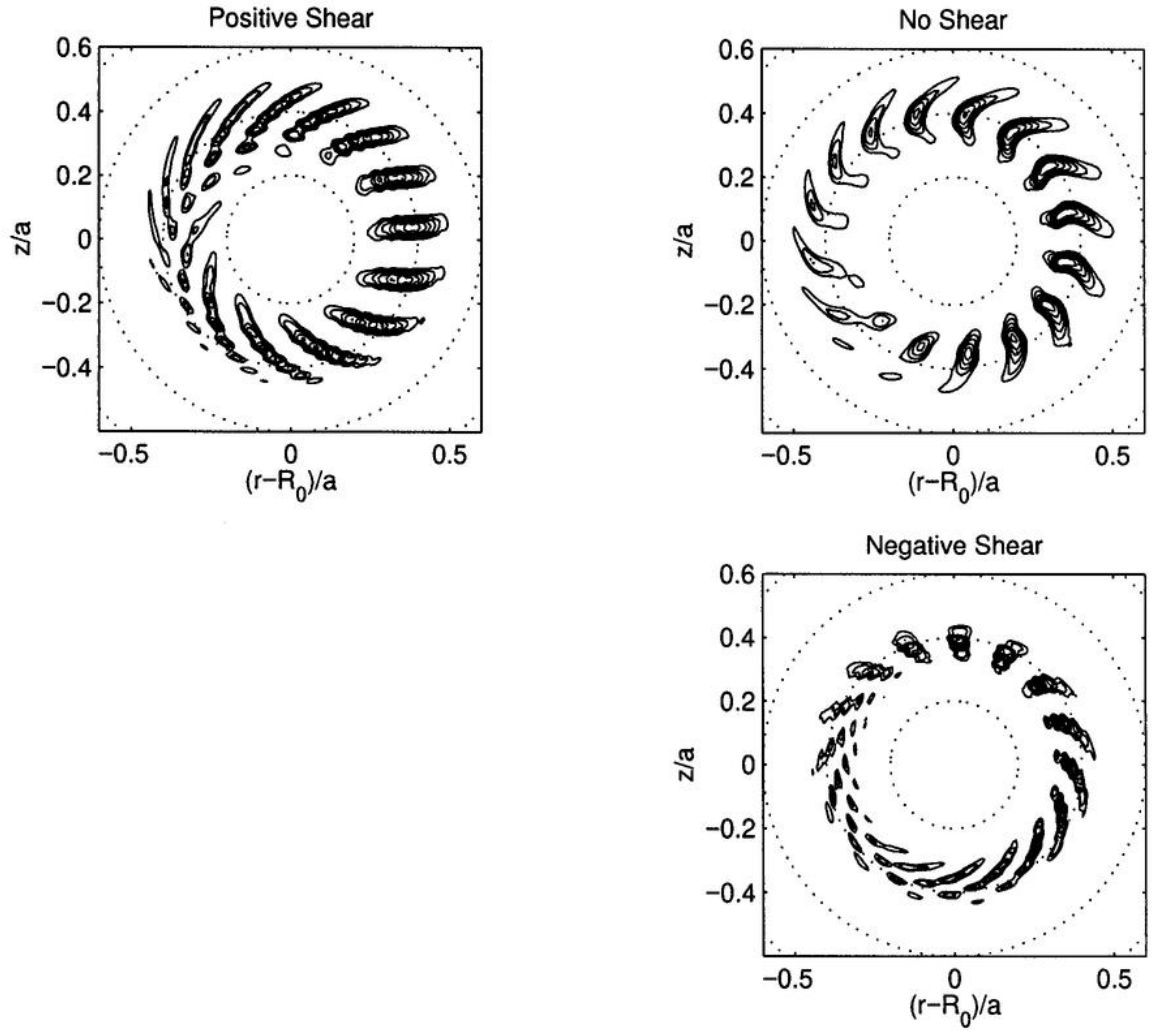

Figure 4.8: Poloidal contours of the ITG modes for the three considered values of magnetic shear.

We now have to choose the profile of $E \times B$ flow that will interest us: we decided to study the effect of the "constant shear" (Eq.4.2) profile on the various values of shear, because it is the most popular one in the literature. In Fig.4.9 we present the evolution of the complete spectrum for increasing values of Mach number.

Before going further, a few comments are mandatory. First, to produce these results, we were obliged to use the "complete scan" method to find the eigenvalues (see the Numerical Implementation section). Moreover, each of the sub-plots in Fig.4.9 required many scans to be produced. To make it short, it must be stressed that these results used a lot of computer resources and took a lot of time to produce.

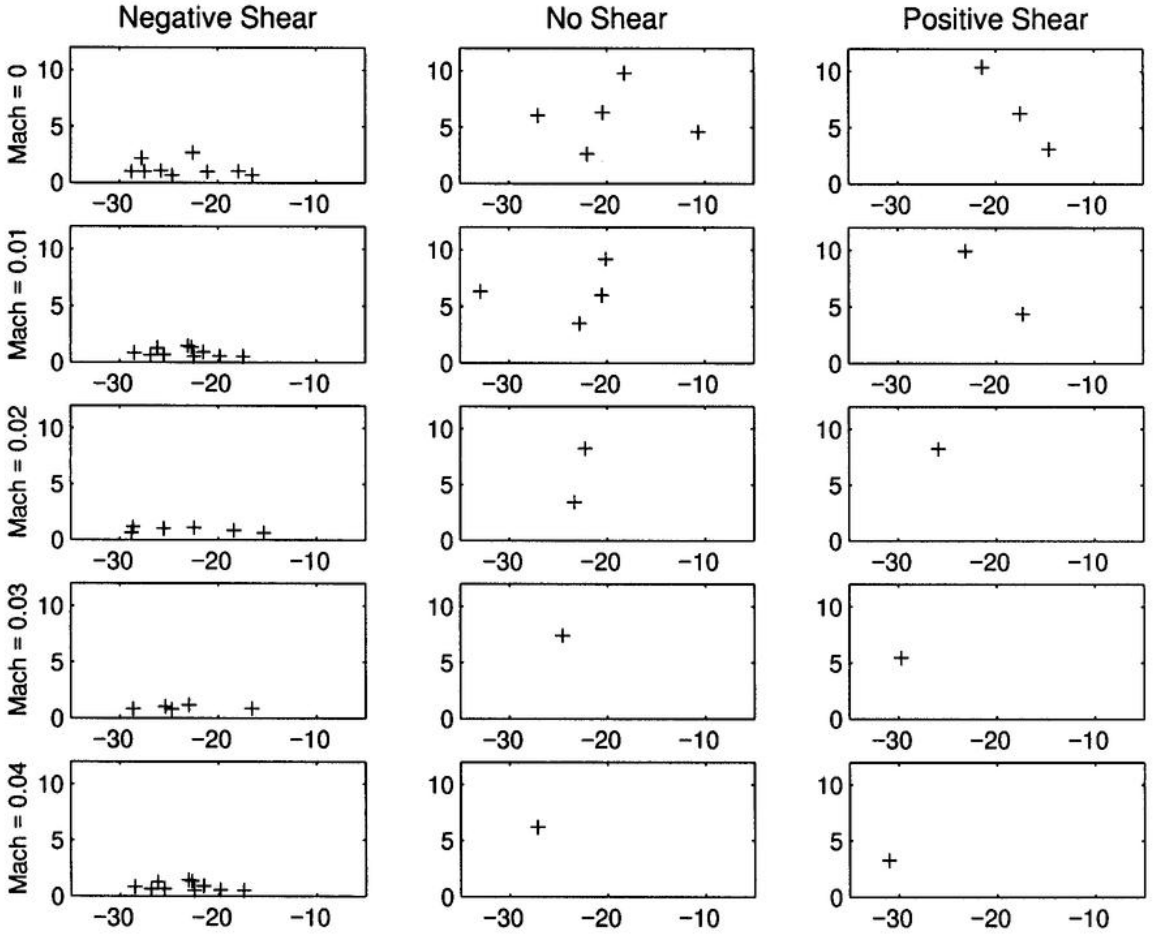

Figure 4.9: Evolution of the complete spectrum in the complex plane (in units of ω_{norm}) as a function of Mach number, for the three magnetic shear cases. Each '+' represents an eigenvalue.

Let us now discuss the results. As is easily observed, the negative shear case is the one presenting the largest number of eigenmodes. This can be understood due to the slab-like nature of these modes. Besides, these modes are clearly less unstable than the other two cases modes, even without flow. But it must also be observed that the effect of $E \times B$ flows in the negative shear case is small. On the other hand, the positive shear case has only a few unstable modes, most of which are quickly stabilized. The no shear case has also only a few unstable modes, most of which are also quickly stabilized, but the most unstable mode in this case is not very strongly affected by flow. These comments are summarized in Fig.4.10, where we plotted only the evolution of the most unstable mode, for the three considered

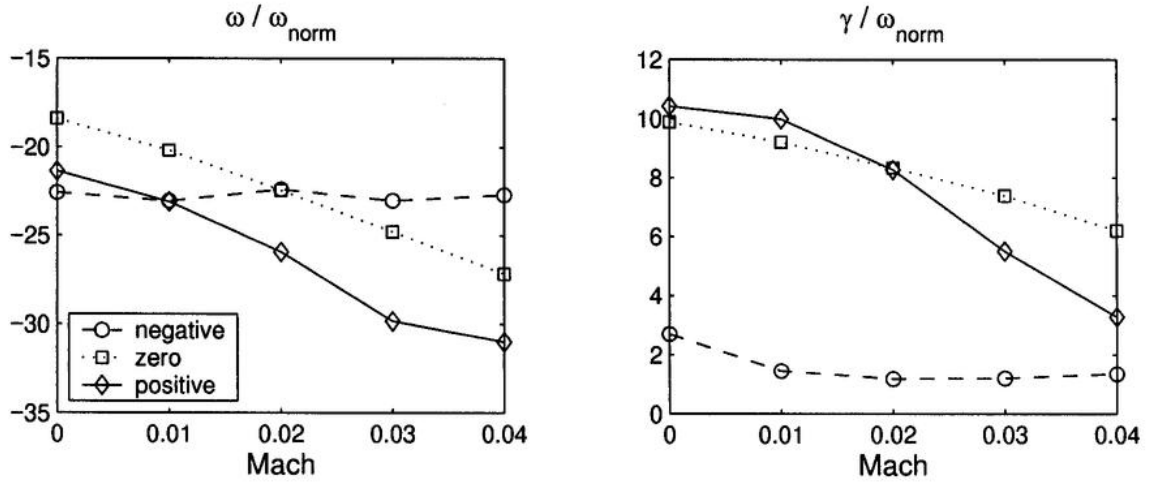

Figure 4.10: Evolution of the most unstable mode for the three considered values of magnetic shear, as a function of Mach number. Circles, squares and diamonds respectively represent the negative, zero and positive magnetic shear cases.

cases. One clearly sees that the negative shear mode stays almost unaffected, while the positive magnetic shear mode is strongly damped. The different evolutions of the frequencies are to be understood by the fact that the radial localization of the modes is not exactly the same for the various shears and therefore the value of flow seen by the mode is slightly different in each case.

How can we understand the observed differences ? If our explanation of the stabilizing mechanism has to be correct, then the differences can be understood in the following way: the positive shear case is a toroidal ITG mode, as it is removed from the region of unfavorable magnetic curvature, its drive is reduced and the mode gets stabilized. On the other hand, the slab-like nature of the negative shear mode allows it to survive without the magnetic curvature, therefore a rotation of this mode will not affect much its growth rate. The conclusion of this study is therefore that there is no synergy between negative shear and $E \times B$ flows.

We would like to say a last word about what could happen if we took negative Mach numbers. The answer is 'nothing particular'. Indeed, as we learned with the first results, there is not much difference on stabilization for different signs of Mach number, the orders of magnitude being exactly the same. Moreover, our

interpretation of why the negative magnetic shear mode is not strongly affected is that, because of its slab-like nature, its rotation in the poloidal plane does not affect much its drive. This would remain true even if we rotated it in the opposite direction. Nevertheless, with more time, one could complete the presented results, running a few negative Mach numbers cases.

4.3 Asdex Upgrade Comparison

So far we had only academic cases with ad-hoc profiles, which in itself is not a problem for me, but many people are eager to see comparisons with experiments. And to be honest, it is certainly interesting to test how good such a simple model as ours can do to catch the important physics. We have therefore decided to study an experimental configuration with our global spectral code. To achieve this, we have collaborated with people of the Asdex Upgrade (AUG) tokamak, in Garching. In particular, the following results would never have been possible without the kind cooperation of Arthur Peeters and Sibylle Günter of the Max Planck Gesellschaft. Thanks to them.

There are two main features to keep in mind for this experimental case. First the shot had an Internal Transport Barrier diagnosed by the AUG experimentalists, which means that the confinement was improved. As we claim that $E \times B$ flows can stabilize microinstabilities, it is thus a good case for us. Second, this case is an ITG mode destabilized by trapped electrons. It is not a pure TEM, because it is still on the frequency side of the ITG modes, but without trapped electrons it would be completely stable.

4.3.1 Equilibrium

The first step to perform for this comparison is to find an AUG shot which suits our needs. We had a choice of several AUG shots where experimentalists had diagnosed an Internal Transport Barrier (ITB). After a little investigation we found a shot

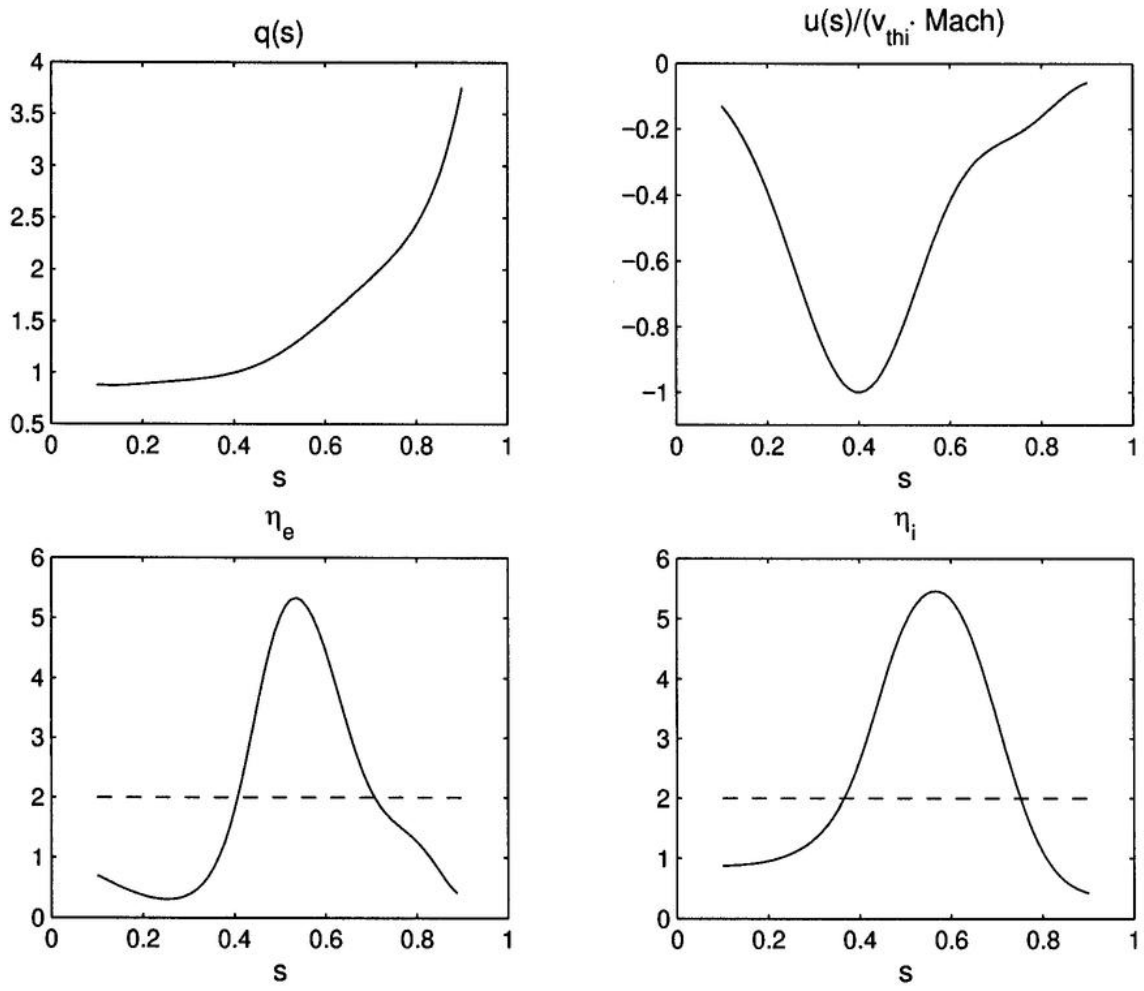

Figure 4.11: Important equilibrium profiles of Asdex Upgrade

which seemed to be an excellent candidate. The experimental reconstructed profiles were introduced as input parameters in our code. The critical profiles are to be seen in Fig.(4.11). The following parameters are also important: $a = 0.51$[m], $R_o = 1.65$[m], $B_o = 2.61$[Tesla], $T_e = 4.56$[keV], $T_i = 13.72$[keV] and the ions are deuterium. One must still decide which n to study: we did a scan in n and took the most unstable mode, which resulted to be for $n = 15$.

These profiles seemed to be smooth enough to avoid numerical problems and had perfectly adequate values of η_e and η_i. Nevertheless, at the beginning we ran into some problems. Indeed, we were first not able to locate any unstable modes, because we had not included the trapped electrons into our calculations. In the

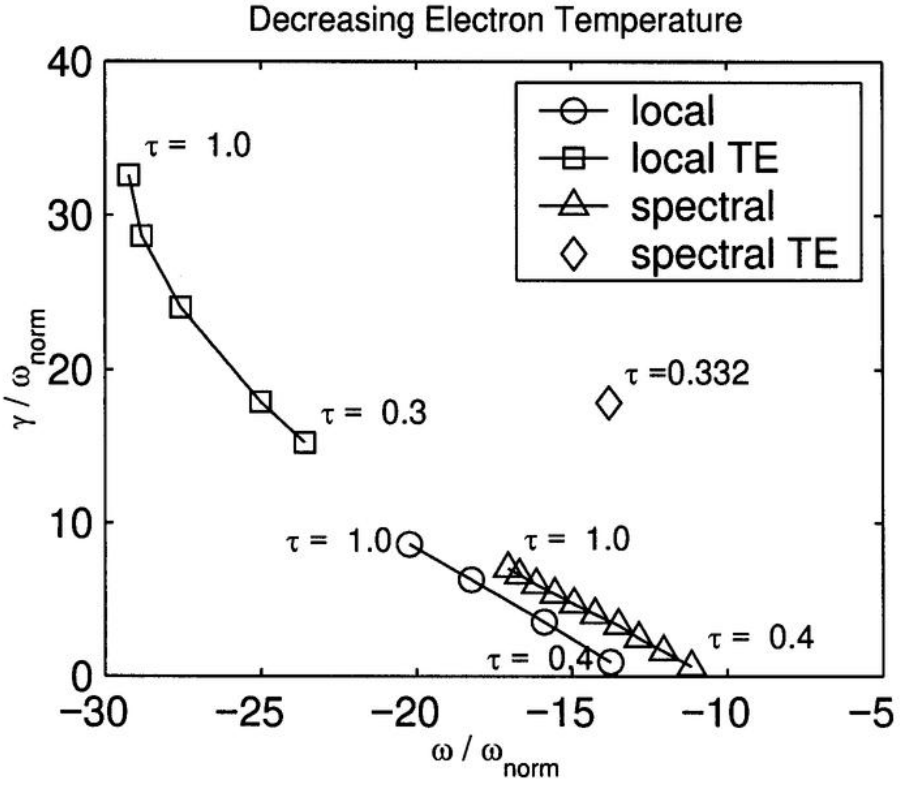

Figure 4.12: Spectrum of the AUG case (without $E \times B$ flows) with and without trapped electrons (TE). The circles and squares are the results of the local dispersion relation, with $\tau = T_e/T_i$ varying from 1 to 0.3 for both cases: with and without TE. the triangles are the evolution of the most unstable global mode without TE and with τ varying from 1 to 0.4. Finally the diamond is the most unstable global mode with TE included, for the experimental value of $\tau = 0.332$. Variations of τ are obtained through the variation of T_e.

somehow too complex Fig.4.12, we explain what happens: the experiment has a value of $\tau = T_e/T_i = 0.332$, that is the ion temperature is roughly three times the electron temperature. Using this value, we did not find any unstable modes, even without $E \times B$ flows. Thus we decided to start with $\tau = 1$ (increasing the electron temperature T_e) and we were then able to find unstable modes. Starting with these modes, we progressively reduced the electron temperature T_e until we reached the experimental value of τ. This resulted in a fast stabilization of the modes. Hopefully, the inclusion of trapped electron effects, starting with $\tau = 1$ and evolving to $\tau = 0.3$, allowed us to find unstable modes even at the experimental value of τ.

This discussion is not meaningless, because it is important to remember that up

to now we did only study how $E \times B$ flows affected the pure ITG modes. This is a case where the main driving force for the instability are the trapped electrons, although this is not a trapped electron mode, as the sign of the frequency did not change.

4.3.2 Diagnostics

This part is due to Arthur Peeters of the IPP Garching. I thank him for taking the time to write the following lines, but of course, I do assume the complete responsibility for what is written here.

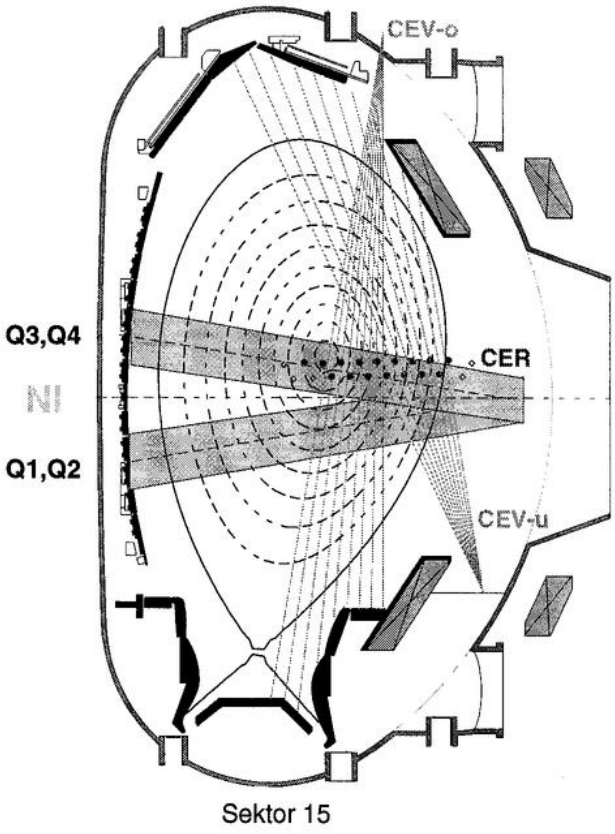

Figure 4.13: Shape of the Asdex Upgrade Tokamak

Electron temperatures are determined with a super-Heterodyne radiometer that measures the emission of electron cyclotron waves for which the plasma is optically thick and therefore the emitted power is proportional to the temperature. The radiometer has a total of 60 channels with different frequencies and consequently

can measure the electron temperature at 60 different positions in the plasma.

The density is obtained from a combined system of lithium beams and an interferometer system. An injected beam of lithium atoms is used to measure the density in the edge of the plasma, whereas the interferometer measure the line averaged density over 8 chords in the plasma and is therefore more sensitive to the central plasma density. The signals of both diagnostics are then used in a combined reconstruction of the density profile

The effective charge is obtained from the emitted Bremsstrahlung of the plasma. A range in the visible light is used to prevent the pick up of line radiation and the diagnostic has a total of 16 chords. The information of other diagnostics (for instance the measured density) is used to calculate the effective charge.

Ion temperature as well as rotation velocities are obtained using Charge Exchange Recombination Spectroscopy. This diagnostic measures the line radiation emitted by charged ions (mostly Carbon) that have received an electron through the collisions with a neutral Deuterium atom. The latter atoms are injected into the plasma for heating. The broadening of the line gives information on the temperature and the Doppler shift can be used to obtain the rotation velocity. The diagnostic measures these quantities at 16 positions in the plasma. The poloidal rotation measurement has rather large error bars and therefore the radial electric field is usually calculated (from the radial force balance) using the neoclassical poloidal rotation.

The q-profile is obtained from a diagnostic that uses the Motion Stark Effect to measure the direction of the magnetic field. A full equilibrium reconstruction is used to transform this information in a q-profile.

The electron temperature and density have typical error bars of around 5%. The ion temperature and the rotation velocities are typically determined within 10% in these cases. Typical error on the safety factor is hard to give. It varies in radius and depends a little on how much you believe in the reconstruction. Let us guess it is around 0.2. For our calculations, however, the largest errors can be expected

in the derived quantities such as the gradient length of the ion temperature and the $E \times B$ rotation velocity. Of course one fits the ion temperature measurements with a smooth curve and then takes the derivative of the smooth curve to obtain the gradient length. The error on this length is then difficult to asses. In principle one could say it is infinite since one can draw curves with an arbitrary gradient length in a certain point which however go through all the measurement points. In some sense the smooth curve is common sense but not necessarily demanded by the measurements. One can only asses the error bars in the gradient lengths already assuming that the working hypothesis of a smooth curve is justified.The values are o.k. within 20% (educated guess). The largest error is in the $E \times B$ shearing rate. This quantity contains second order derivatives of the profiles, and the poloidal rotation velocity which is not determined very well. Happily this quantity is dominated by the toroidal rotation velocity (around $s = 0.6$) which is determined with some accuracy. Nevertheless, the estimated error can be as large as 40%. All the error bars given above are rather rough estimates. To some extent, they are connected with a belief rather than solid physics.

4.3.3 Spectrum

We can now show how the $E \times B$ flows affect the AUG spectrum. In Fig.4.14 we present the complete spectrum of the AUG case, with trapped electrons, for three increasing values of Mach number. It is clear that the number of modes is decreasing with increasing Mach number, as is the maximum growth rate. It must be stressed that in this particular case, the most instable mode is not always the same. This is due to the fact that the various unstable modes do not have the same radial profile and thus do not see the same part of the $E \times B$ profile. This results in Doppler shifts of various amplitudes, and the stabilizing mechanisms, whether the value of flow or its first derivative, are different for each mode.

In Fig.4.15 we present the most unstable mode in the poloidal plane, with and

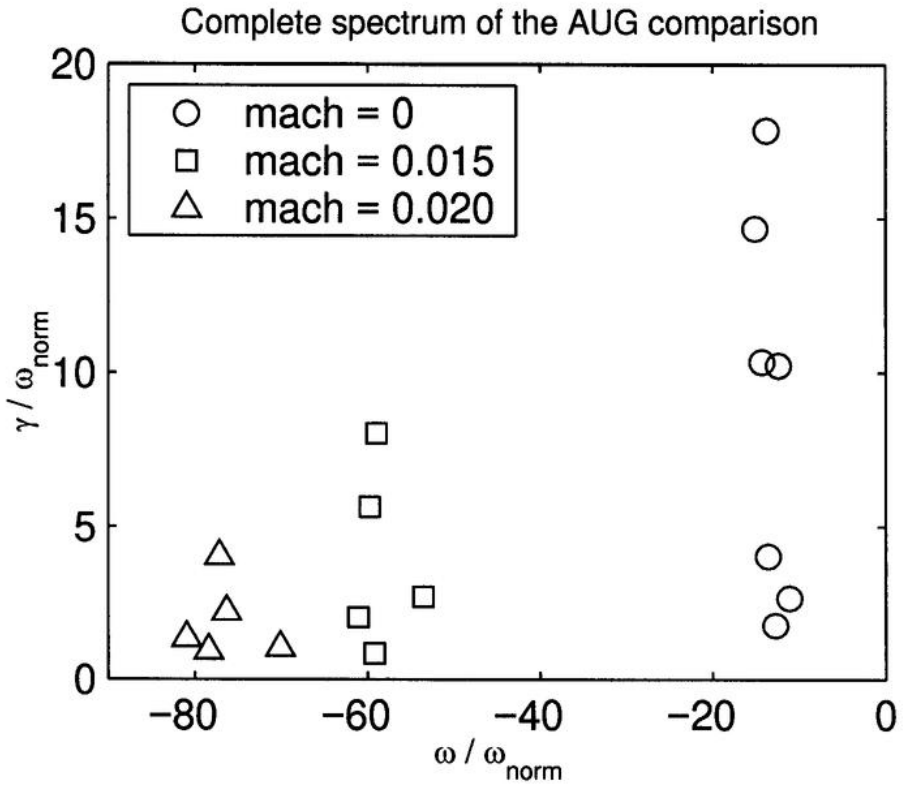

Figure 4.14: Complete spectrum of the microinstabilities of the AUG case, for various value of Mach number: circles are global results without flow, while squares and triangles represent increasing values of Mach number.

without $E \times B$ flows. As we see, the ballooning region θ_o is not rotated in this

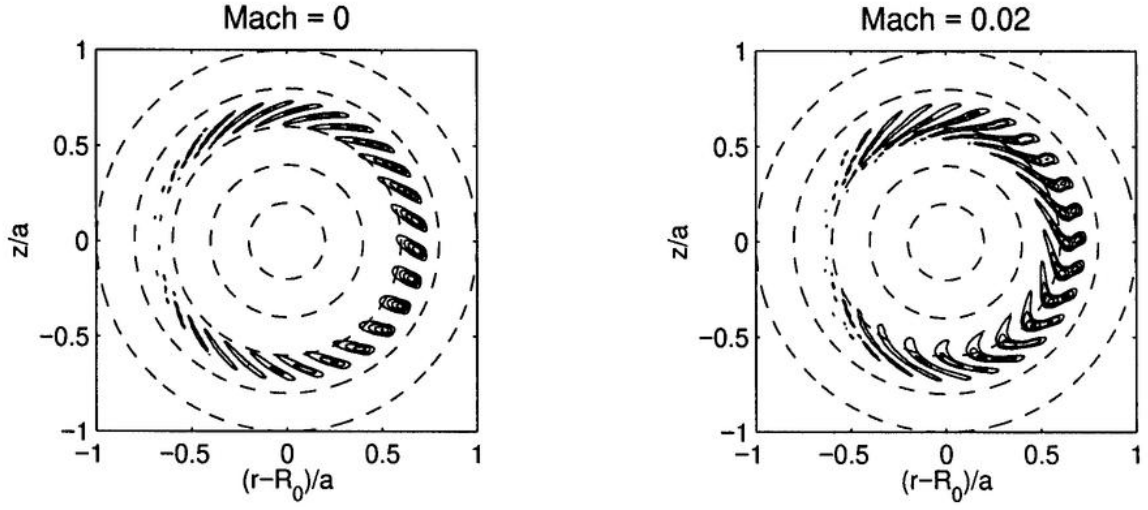

Figure 4.15: Most unstable mode of the AUG spectrum, without and with $E \times B$ flow.

case. Therefore our previous argument to explain stabilization seems no longer valid. First, let us remember that we are not observing the same mode in the two pictures: each mode is the most unstable for the given Mach number, but these are two different modes. Thus, it might be that for one given mode the θ_o region changes, but that the most unstable mode has it always close to $\theta \approx 0$. Second, we must remember that the modes we are studying are not pure ITG modes, as if we had not included the trapped electrons, the spectrum would have been stable. Therefore, as $E \times B$ flows have been neglected in the construction of the trapped electron contribution (due to the mass ratio), it is by no means simple to understand how they affect the present modes. To be clear, the $E \times B$ flows affect only the passing ions contribution to the mode, but without the trapped electron contribution there would be no mode. But the passing ions contribution is also essential to the mode, as it is not a TEM mode, but an ITG mode destabilized by trapped electrons. Therefore, it might well be possible that the poloidal structure of the mode is dictated by the trapped electrons, thus barely affected by $E \times B$ flows. But $E \times B$ flows still stabilize the mode, because they reduce the passing ions contribution, which is also essential to the existence of the mode.

Let us now come to the comparison with the experimental observations. With our results we seem to observe that for a theoretical value of Mach number close to 0.03:

$$\text{Mach}_T \approx 0.03 \tag{4.2}$$

we will have completely stabilized the AUG spectrum. Now comes the question of how large is the experimental value of Mach number. It turns out that the measured Mach number is:

$$\text{Mach}_E = 0.0635 \tag{4.3}$$

As a first comment, I would like to say that it was already very good news to discover that the orders of magnitude were right. Then, I would stress another point: the theoretical value of Mach number represents the value by which the

linear microinstabilities should be stabilized, it does not represent a maximum on the value of Mach number. What I mean is that it would have been more annoying if the theoretical value had been larger than the experimental one, as then experimentalists would claim an ITB where theorists would see none. But in our case, there is no argument why the Mach number could not be larger than the minimal stabilization value, represented by the theoretical value. Moreover, there are many limitations of both theory and experiment.

Theory is limited by:

- unrealistic shape of the equilibrium, which strictly speaking is not even an MHD equilibrium
- only linear calculations
- no electromagnetic effects
- the other (less obvious) approximations used in the code

Experimental values must be taken with care:

- an error bar of 20% on the ion temperature gradient
- an error bar of 40% on the $E \times B$ flows

These limitations seem more than sufficient as explanations. They even are so strong, that there is a valid reason to doubt that our results are due to good physics. The only way to address this doubt would be to simulate more experimental shots, but this was not possible in the available time.

4.4 Conclusion

The first global and kinetic study of $E \times B$ flows on the linear stability of ITG modes has been presented. It shows that:

- $E \times B$ flows have a very strong stabilizing effect on toroidal ITG modes.

- Only the intensity of the flow and its first derivative have an effect.
- For instance, the second derivative of flow (or curvature of flow) does not have any relevant effect.
- Negative magnetic shear does not enhance the effect of $E \times B$ flows.
- On the contrary, modes with positive magnetic shear are the most sensitive to $E \times B$ flows.
- Computed values are in qualitative and quantitative agreement with the only simulated experiment.

This closes the results part of this PhD. There remains a lot of work to be done with this model: the next step already underway is the inclusion of trapped ions with $E \times B$ flows. Then the most important step will be inclusion of electromagnetic effects in the model and this is already in construction.

I think we can now safely proceed to the general conclusion of the work.

Chapter 5

Conclusion

We have now reached the end of this four years work. Although this book is already a summary of my work, I will now summarize this summary. So, we undertook the study of the effect of $E \times B$ flows on linear global microinstabilities. The main features of this work are: a global resolution, which is needed to study this effect, a spectral approach and ad-hoc equilibrium quantities.

The main result is that the simple value of the radial electric field is at least as important as the value of its first derivative. This is a simple linear phenomenon which is quite easily understood: toroidal ITG modes need unfavorable magnetic curvature to exist and the simple value of the radial electric field induces a poloidal rotation of the plasma and of the mode, thus removing it from its main drive region.

Nevertheless, the usually summoned explanation for stabilization is not invalidated: the shear of the radial electric field produces a decorrelation of the mode structure, thus leading to stabilization. But this mechanism is mainly non-linear, while our result is simply linear. However, it was nice to find a simple new linear mechanism for stabilization.

Other results include a study of $E \times B$ flows interaction with negative magnetic shear, which was not very conclusive. It showed that in our simple model there is no miraculous effect of a negative magnetic shear. Eventually, we conducted a comparison with the Asdex Upgrade tokamak in Garching, which produced a good agreement, although I do have some difficulties in trusting this too much, as our

model is far too simple to produce any meaningful description of an experiment. Not to mention the experimental error bars on absolutely critical parameters for our code.

I would like now to say a word about what remains to be done with this code. First of all, study of the effect of $E \times B$ flows on trapped ion modes. The equations are ready since a long time and the results almost made it to this PhD, but not quite ! This will be produced very soon. Then, a very fundamental part of the physics is missing for the moment: the electromagnetic effects. These effects are vital, especially for any meaningful comparison with an experiment. Their inclusion in our model is currently underway by another PhD student. Finally, in a more general perspective, there remain many open questions about $E \times B$ flows: how are generated the strong radial electric fields ? Does the system non-linearly saturate to a new steady state ? And if yes, how is this state different ? But this is altogether another story.

Bibliography

[1] L.I.Rudakov, R.Z.Sagdeev, Nuclear Fusion Suppl.1962 **2**, 481, (1962)

[2] P.Terry, W.Anderson, W.Horton, Nuclear Fusion **22** (4), 487, (1982)

[3] W.Horton, Duk-In Choi, W.M.Tang, Phys.FLuids **24** (6), 1077, (1981)

[4] E.A.Frieman, G.Rewoldt, W.M.Tang, A.H.Glasser, Phys.Fluids **23** (9), 1750, (1980)

[5] F.Romanelli, Phys.Fluids B **1** (5), 1018, (1989)

[6] X.Garbet, L.Laurent, F.Mourgues, J.P.Roubin, A.Samain, X.L.Zou, J.Chinardet, Phys.Fluids B **4** (1), 136, (1992)

[7] J.Q.Dong, W.Horton, J.Y.Kim, Phys.Fluids B **4** (7), 1867, (1992)

[8] R. Marchand, W.M. Tang, G. Rewoldt, Physics of Fluids **23**, 1164 (1980)

[9] S.Brunner, J. Vaclavik, Physics of Plasmas **5**(2), 365, (1998)

[10] S.Brunner, M. Fivaz, T.M. Tran and J. Vaclavik, Physics of Plasmas **5**(11), 3929, (1998)

[11] K.H. Burrell, Plasma Phys. Controlled Fusion **36**, A291 (1994)

[12] K.H. Burrell, Phys. Plasmas **4**, 1499 (1997)

[13] K.H. Burrell, Phys. Plasmas **6** (12), 4419 (1999)

[14] J.W. Connor and H.R. Wilson, Plasma Phys. Controlled Fusion **43**, R1 (2000)

[15] G.M. Staebler and R.R. Dominguez, Nucl. Fusion **31** (10), 1891 (1991)

[16] X.-H. Wang, P.H. Diamond and M.N. Rosenbluth, Phys. Fluids B **4** (8), 2402 (1992)

[17] B.I. Cohen, T.J. Williams, A.M. Dimits and J.A. Byers, Phys. Fluids B **5** (8), 2967 (1993)

[18] R.E. Waltz, R.L. Dewar and X. Garbet, Phys. Plasmas **5** (5), 1784 (1998)

[19] G. Rewoldt, M.A. Beer, M.S. Chance, T.S. Hahm, Z. Lin and W.M. Tang, Phys. Plasmas **5** (5), 1815 (1998)

[20] J.B. Taylor, H.R. Wilson, Plasma Phys. Control. Fusion **38**, 1999, (1996)

[21] S. Sen and R.G. Storer, Phys. Plasmas **4** (9), 3113 (1997)

[22] S. Sen, P.K. Sharma and D. Bora, Phys. Plasmas **5** (7), 2637 (1998)

[23] T.S. Hahm, Phys. Plasmas **1** (9), 2940 (1994)

[24] T.S. Hahm and K.H. Burrell, Phys. Plasmas **2** (5), 1648 (1995)

[25] T.S. Hahm, Phys. Plasmas **4** (11), 4074 (1997)

[26] G. Ganguli, Phys. Plasmas **4** (5), 1544 (1997)

[27] J.Y. Kim and Y. Kishimoto, Phys. Plasmas **3** (10), 3689 (1996)

[28] M. Maccio, J. Vaclavik and L. Villard, in *Theory of Fusion Plasmas, Int. Workshop, Varenna, September 1998* (Editrice Compositori, Società Italiana di Fisica, Bologna, 1999), p.511

[29] T.S. Hahm, Physics of Fluids **31**, 2670 (1988)

[30] S. Brunner and M. Fivaz, in *Theory of Fusion Plasmas, Int. Workshop, Varenna, August 1996* (Editrice Compositori, Società Italiana di Fisica, Bologna, 1996), p.101

[31] B. Davies, Jour. Comp. Phys., **66**, 36 (1986)

[32] M. Fivaz, Comp. Phys. Comm., **111**, 27 (1998)

[33] J.R. Cary and R.G. Littlejohn, Ann. Phys., **151**, 1 (1983)

Acknowledgments

The content of this PhD is definitively my work, but I now would like to thank a few persons that made this work easier and a person who made it possible.

To start with the ones who helped me, I would like to express my gratitude to my fiancée, Isabelle. She sustained me through all the ups and downs of this work and simply made my life more enjoyable. Merci. Then I would like to say a word about my parents: their caring love and attention allowed me to concentrate on my work. Grazie. And last, I wish to thank my PhD director, Laurent Villard, for his kind support. Merci.

And now a word about the person who made this PhD possible: Jan Vaclavik. I first met him during my fourth year of study and he guided me through my diploma. He had the idea of this research and gave me the opportunity to work on it. Thank you for leading me to the end of this PhD and for all the time you spent trying to make a physicist of me.

Curriculum Vitæ

I was born in Italy, Rome, in 1972. My parents moved to Switzerland in 1977 and I did all my studies in the swiss public school. In 1991 I received my 'Maturité fédérale' and proceeded to study physics in the swiss federal institute of technology, Lausanne (EPFL). I graduated in 1996 and I am a PhD student in the CRPP since then. Today, I am 27 years old and will try to defend my PhD.